Benefits of therapy by dynamin-2-mutant-specific silencing are maintained with time in a mouse model of dominant centronuclear myopathy

Delphine Trochet, Bernard Prudhon, Lylia Mekzine, Mégane Lemaitre, Maud Beuvin, Laura Julien, Sofia Benkhelifa-Ziyyat, Mai Thao Bui, Norma Romero, Marc Bitoun

Benefits of therapy by Dynamin 2 mutant specific silencing are maintained with time in a mouse model of dominant centronuclear myopathy

Delphine Trochet[1], Bernard Prudhon[1], Lylia Mekzine[1], Mégane Lemaitre[2], Maud Beuvin[1], Laura Julien[1], Sofia Benkhelifa-Ziyyat[1], Mai Thao Bui [3], Norma Romero[1,3], Marc Bitoun[1]

1. Sorbonne Université, Inserm, Institut de Myologie, Centre de Recherche en Myologie, F-75013 Paris, France.

2. Sorbonne Université, Inserm, UMS28, F-75013 Paris, France.

3. Neuromuscular Morphology Unit, Myology Institute, GHU Pitié-Salpêtrière, 75013, Paris, France.

*Corresponding authors: d.trochet@institut-myologie.org or m.bitoun@institut-myologie.org

Running title: Long-term maintenance of allele-specific therapy for *DNM2*-myopathy

Abstract

Dominant dynamin 2 (DNM2) mutations are responsible for the autosomal dominant centronuclear myopathy (AD-CNM), a rare progressive neuromuscular disorder ranging from severe neonatal to mild adult forms. We previously demonstrated that mutant-specific RNA interference is an efficient therapeutic strategy to rescue the muscle phenotype at the onset of the symptoms in the AD-CNM Knock-in-*Dnm2*$^{R465W/+}$ mouse model. Our objective was to evaluate the long-term benefit of the treatment along with the disease time course. We demonstrate here that the complete rescue of the muscle phenotype is maintained for at least one year after a single injection of adeno-associated virus expressing the mutant specific shRNA. This was achieved by a maintained reduction of the mutant *Dnm2* transcript. Moreover, this long-term study uncovers a pathological accumulation of DNM2 protein occurring with age in the mouse model and prevented by the treatment. Conversely, a physiological DNM2 protein decrease with age was observed in muscles from wild-type mice. Therefore, this study highlights a new potential pathophysiological mechanism linked to mutant protein accumulation and underlines the importance of DNM2 protein expression level for proper muscle function. Overall, these results strengthen the allele-specific silencing approach as a robust, safe, and efficient therapy for AD-CNM.

Introduction

Autosomal dominant centronuclear myopathy (AD-CNM, MIM #160150) is a rare congenital myopathy characterized by progressive muscle weakness, mainly affecting limb and facial muscles. Age of onset and severity of symptoms are variable ranging from severe-neonatal to mild-adult forms.[1] Histological hallmarks in muscle biopsies consist of nuclear centralization in absence of regenerative process associated with atrophy and predominance of type 1 fibers and radial arrangement of sarcoplasmic strands radiating from the central nuclei.[1] AD-CNM results from heterozygous mutations in the *DNM2* gene which encodes dynamin 2 (DNM2)[2,3] and to date thirty-seven mutations (mainly missense) have been identified.[2,4–11] Dominant *DNM2* mutations also cause rare cases of Charcot-Marie-Tooth peripheral neuropathy (CMT, MIM #606482)[12] and hereditary spastic paraplegia.[13] DNM2 belongs to the superfamily of large GTPases and is involved in endocytosis and intracellular vesicle trafficking through its role in deformation of biological membranes by oligomerization at the neck of membranes invagination leading to the release of vesicles.[14,15] Furthermore, several studies have highlighted the role of DNM2 as a regulator of actin and microtubule cytoskeletons.[15,16]

DNM2 mutations in AD-CNM are thought to lead to a gain of function and/or a dominant negative effect through the potential formation of abnormal stable DNM2 oligomers associated with mis-regulated GTPase activity.[17,18] In addition, absence of haploinsufficiency in AD-CNM is supported by data from patients and absence of phenotype developed by heterozygous knock-out mice expressing 50% *Dnm2*.[19,20] Consequently, AD-CNM fulfils all the criteria for the development of allele-specific silencing therapy by RNA interference (RNAi) devoted to silence the mutated mRNA without affecting the normal transcript.[21] Indeed, we have established the proof-of-concept of allele-specific RNA silencing therapy in a knock-in mouse model of *DNM2*-linked CNM (KI-*Dnm2*$^{R465W/+}$) and patient-derived cells.[22] The KI-*Dnm2*$^{R465W/+}$ mouse model (thereafter called KI-*Dnm2*^{R465W}) harbors the most frequent *DNM2*-

CNM mutation (30% of AD-CNM patients) and progressively develops features of the human disease including impairment of force generation, muscle atrophy and morphological abnormalities of the muscle fibers.[23] We showed that adeno-associated virus (AAV)-mediated allele-specific RNAi targeting the R465W mutant allele is able to completely prevent this muscle phenotype in young mice while partially restore muscle function in older mice probably due to a viral transduction defect.[22] In the present study, we aim at establishing the long-term benefit of mutant-specific silencing after a single AAV-shRNA injection in young KI-*Dnm2*^{R465W} mice and to improve the treatment efficacy in older mice.

Results

Therapeutic benefit on muscle phenotype is maintained long-term

To assess the long-term maintenance of phenotype restoration, a single intramuscular injection of AAV1 expressing or not the R465W mutant-specific shRNA (i.e. AAV1-sh9 and AAV1-control) was performed in tibialis anterior muscle (TA) of the KI-*Dnm2*^{R465W} mice at 1 month of age (10^{11} viral genomes (vg)/TA) and mice were sacrificed after 1 year. Heterozygous (HTZ) KI-*Dnm2*^{R465W} mice received the therapeutic AAV1-sh9 in the right TA and AAV1-control in the contralateral muscle. The wild-type (WT) mice received the AAV1-control in the left muscle and PBS in the contralateral muscle.

A 18% reduction in muscle mass was observed in untreated HTZ muscle while a single injection of AAV-sh9 restored muscle mass close to WT values (Figure 1A). Measurement of fiber diameter performed on transversal TA sections immunolabelled with Laminin antibody showed a reduced mean fiber size in HTZ muscle compared to WT which was corrected in the treated muscle (Figure 1B). In addition, fiber size distribution in the treated muscle was similar to the WT with the exception of persistence of medium-sized fibers and a slightly lower number of large fibers (Figure 1C and SupS1). Muscle histopathology was studied on transversal TA sections stained with hematoxylin and eosin (HE), succinate dehydrogenase (SDH), and reduced diphosphopyridine nucleotide diaphorase (DPNH) (Figure 1D and SupS2). The disease-specific histopathological abnormalities, *i.e.* central accumulation of oxidative cell compartments within fibers, were observed in 18% of fibers in HTZ control muscles and absent in AAV1-sh9 treated muscles (Figure 1E, shown by asterisks in Figure 1D). Moreover, global DNPH and SDH staining in entire muscle section showed an increased oxidative staining in the posterior region of the untreated HTZ muscles compared to WT which was also abolished in AAV1-sh9 treated muscles (Fig SupS2). Absence of myofiber with central nuclei in HE confirmed that the AAV-sh9 was not toxic and did not induced muscle degeneration (Figure

1D lower panel). Transient activation of the ubiquitin-proteasome and autophagy pathways was previously demonstrated in the heterozygous Knock-in model at 2 months of age.[23] Therefore, we assessed the expression of Gabarapl1, p62, Atg 4, Murf1, and Atrogin 1 in the TA muscle of the 13-month-old mice by RT-qPCR. With the exception of p62 expression which slightly decreased in HTZ mice, we found similar expression of all genes in untreated WT and HTZ mice, whereas Murf1 and Gabarapl1 expression decreased in heterozygous treated mice (Fig SupS3). We have recently reported a reduction of the satellite cell content in muscle of KI-*Dnm2*^{R465W} mice associated with a decreased expression of *Pax7*.[24,25] Therefore, we analyzed *Pax7* expression in TA muscles from WT, HTZ-control and HTZ-sh9 treated mice by quantitative real-time PCR and immunostaining. We confirmed a decrease of ~60% in *Pax7* expression in HTZ-untreated muscle compared to the WT by qPCR and *Pax7* expression was not improved in the AAV1-sh9 treated HTZ mice (Figure 1F and Fig SupS4). Finally, force measurements showed that absolute and specific forces were significantly reduced in TA muscle from untreated HTZ mice (-30% and -20%, respectively) and were restored to normal values in treated HTZ mice (Figures 1G and 1H). Overall, these results showed a long-term benefit of allele-specific silencing therapy since muscle mass, morphology and function were maintained one year after a single injection of the therapeutic AAV.

Viral genome persists in HTZ muscle after a 1-year treatment

We measured persistence of AAV in HTZ and WT muscles after 1 year through quantification of viral genomes (vg) per nanogram of genomic DNA. A similar amount of vg was found in HTZ muscles injected with AAV1-sh9 and AAV1-control (960 vg/ng) (Figure 2A) also supporting absence of toxicity of the long-term expression of the sh9 RNA and a similar persistence of both virus in HTZ muscles. In contrast, AAV1-control values were almost tenfold higher in WT muscle (~8800 vg/ng) (Figure 2A). We looked at potential immune response induced in HTZ muscle by long-term expression of shRNA through the potential

induction of interferon response by semi-quantitative RT-PCR. Similar expression of two interferon-induced genes (*Oas1* and *Stat1*) was observed in HTZ-control, HTZ-sh9 and WT muscles (Figure 2B) ruling out abnormal immune response in HTZ muscles. This result along with absence of fibrosis and signs of muscle necrosis-regeneration in HE-stained muscle sections (Figure 1D) confirmed safety of long-term expression of the therapeutic molecule. In addition, given that viral genome amount 1 month after AAV injection were comparable between 1-month-old WT and HTZ mice (Fig. SupS5), our results also suggested a partial loss of viral genome in the HTZ muscle with time independent of muscle regeneration but without significant impact on the therapeutic benefit at one year.

Specific silencing of mutated allele is maintained over time

Expression of *Dnm2* transcript was quantified by semi-quantitative RT-PCR normalized with ATPase transcript. A significant decrease in the *Dnm2* mRNA content was observed in sh9-expressing HTZ muscle compared to untreated HTZ and WT muscles (-20%) (Figure 3A) and confirmed by qPCR (Fig. SupS6A). Allele-specific silencing was checked using *Dnm2* RT-PCR and EcoNI enzymatic digestion to discriminate mutated (undigested) from WT allele (digested) (Figure 3B). A significant decrease of mutant/WT ratio was observed in treated muscle (-30%) due to specific silencing of the mutant transcript and unchanged expression of the WT *Dnm2* mRNA (Figure 3B). A second RT-PCR assay using primers designed for specific amplification of either WT or mutant alleles confirmed these results (Fig. SupS6B). The DNM2 protein expression was then quantified using western blot and densitometric analysis. In untreated HTZ muscles, a two-fold increase in DNM2 expression was observed compared to WT muscles while DNM2 expression was similar in WT and HTZ treated muscle (Figure 3C). Altogether, these data demonstrated that allele-specific silencing was maintained 1 year after a single AAV1-sh9 intramuscular injection. These results also highlighted an age-related

accumulation of the DNM2 protein without increase in mRNA expression in muscle of HTZ mice at 1 year of age.

Dynamin 2 protein is down-regulated with age in normal mouse muscle

The increased DNM2 protein expression in HTZ muscles compared to WT muscles of 13-month-old mice (Figure 3C) suggested a change of DNM2 expression with age. To test this hypothesis, we investigated the DNM2 expression in TA muscles from WT and HTZ KI-*Dnm2*^{R465W} mice at 1 month, 3 months and 6 months of age using western blot (Figure 4A). In WT muscle, the DNM2 content remained stable between 1 and 3 months and was then decreased by half at 6 months of age. In HTZ muscle, the DNM2 protein content was higher at 1 month of age compared to WT, and returned to amount comparable with WT in 3-month-old mice, in accordance with previous observation at this age.[26] Then, between 3 and 6 months of age, the DNM2 protein content remained stable in HTZ muscle, leading to a 2-fold higher protein content compared to WT at 6 months of age. Together these data support a physiological decrease in DNM2 protein content in wild-type muscle from 3 to 6 months of age which was impaired in presence of the R465W DNM2 mutation.

We then investigated whether this physiological decrease of DNM2 occurred at transcriptional level by quantifying *Dnm2* mRNA in tibialis anterior muscle in 1- and 9-month-old mice using semi-quantitative RT-PCR. As shown in Figure 4B, the level of *Dnm2* mRNA was similar in these muscles regardless of the age and genotype. Therefore, as for the accumulation of mutant protein observed in mutant muscle (Figure 3C), the physiological decrease of DNM2 protein content in WT muscle results from post-translational event which is altered in HTZ mice.

We then wondered if the physiological decrease in DNM2 protein content with aging in WT mice was muscle-specific. We investigated the DNM2 expression in several muscles (quadriceps, gastrocnemius, and heart) and non-muscle tissues (liver and brain) from WT mice

at 1 and 9 months of age using western blot (Figure 4C). DNM2 protein content was quantified by densitometry and normalized with total protein detected by Stain-Free. In WT brain and liver, no significant decrease in DNM2 protein expression was highlighted with age (Figure 4C, $p = 0.82$ and 0.41 respectively). In muscle tissues, while the significance threshold is not reached ($p=0.057$ for all of them), we observed a decrease in DNM2 protein amount between 1 and 9 months with a more important decrease in quadriceps and gastrocnemius muscles than in heart.

DNM2 protein content was also compared between WT and HTZ mice at the age of 9 months (Fig. SupS7). No difference was found between the two genotypes in brain and heart while an increase in protein content was observed in quadriceps and gastrocnemius but below the significant threshold ($p=0.057$). Altogether these results supported a skeletal muscle-specific physiological decrease of DNM2 protein with age in WT mice that would be impaired in HTZ mice.

Dynamin 2 expression is also down-regulated with age in healthy human muscle

We then investigated the relevance of age-related variation in DNM2 protein in human. To this end, we assessed DNM2 expression in muscle biopsies from healthy subjects and CNM patients at various ages (ranging from 1 month to 60 years old) by western blot (Figure 5A). For analysis, we grouped the control samples as younger or older than 20 years old ($n=6$ for both group, Figure 5B). We observed that DNM2 expression was ~30% lower in the older group compared with the younger ($p<0.05$). Moreover, when plotting individual DNM2 expression level as a function of age, we observed a negative correlation ($r=-0.7$, $p<0.05$) in controls samples. Considering CNM samples, spearman correlation was non-significant ($r=0.70$, $p=0.17$) and the number of patients was not sufficient to constitute a group of age, however at matched aged we observed a level of DNM2 that tends to be higher in CNM patients (Figure 5C and SupS8).

High dose of therapeutic AAV does not improve the transduction defect occurring in old mice

We previously highlighted a viral transduction defect in 6-month-old mice compared to 1-month-old HTZ mice explaining the lower efficacy of the treatment in old mice.[22] Therefore, we wanted to explore the possibility to improve treatment efficacy in old mice by using a 10-fold increase in therapeutic AAV1-sh9 compared to the dose used in our previous study (10^{11} vg/TA). A single intramuscular injection was performed in TA of HTZ mice at 6 months of age (10^{12} vg/TA). HTZ mice received an AAV1-sh9 in the right TA and PBS in the contralateral muscle. The WT mice received only PBS in both TA since such amount of virus in a WT mouse muscle leads to muscle regeneration. Mice were sacrificed after 3 months to perform molecular analysis and force measurements. We did not show significant variation in the total *Dnm2* transcript in treated mice and only a slight reduction of the mutant transcript (Figure 6B). As already reported with a lower dose[22], a significant improvement of contractile properties occurred but muscle mass was unchanged (Figure 6A). We then evaluated the viral genome amount in HTZ muscles injected with high dose of virus (10^{12} vg/TA) in comparison with HTZ muscle samples injected with low dose of virus (10^{11} vg/TA). We found 382 vg/ng of DNA in the latter muscles *versus* 1055 vg/ng in muscle injected with the tenfold higher dose (Figure 6C). A virus loss subsequent to muscle regeneration due to potential toxicity was ruled out by absence of central nuclei observed in HE staining (Figure 6D). Overall, despite improvement of muscle contractile properties, a 10-fold increase of therapeutic AAV1-sh9 was unable to by-pass the transduction defect in 6-month-old KI-*Dnm2* mice.

Discussion

High efficacy and specificity of RNA interference (RNAi) to silence morbid genes have been at the origin of numerous clinical trials. These two properties of RNAi have been also used to specifically target the mutated allele without affecting the normal allele in dominant inherited diseases even when the two sequences only differed by one nucleotide. Proof of concept of allele-specific RNAi (AS-RNAi) was achieved for almost 20 diseases in patient-derived cells and/or animal models including the *DNM2*-linked dominant centronuclear myopathy.[21,22] Here, we addressed a key point for preclinical development of AAV-mediated therapy for AD-CNM which is the long-term maintenance of therapeutic benefit *in vivo*.

The long-term expression of transgene is one of the advantage of AAV delivery as transgene expression has been detected up to 10 years after single injection in non-dividing tissues.[27] However, a decrease of transgene expression starting from 7 months after AAV injection in mice has been also reported.[28] To the best of our knowledge, only one study addressed the long-term maintenance of AAV-mediated AS-RNAi therapy *in vivo* showing a decrease in treatment benefit with time in a mouse model of cardiomyopathy through an undetermined mechanism[29] highlighting a potential limitation for the preclinical development of this therapy. Here, we report a rescue of muscle mass, force and histological phenotypes developed by the heterozygous KI-*Dnm2*^{R465W} mice[23] one year upon a single AAV1-sh9 injection performed at the beginning of symptoms demonstrating the long-term maintenance of the therapeutic benefit previously demonstrated after a 3-month treatment.[22] Specific reduction of *Dnm2* mutant is therefore able to revert the impairment of the muscle contractile properties and prevent the development of muscle atrophy and histological features. In addition, we confirmed in TA muscle the decreased expression of the *Pax7* satellite cells marker previously reported in gastrocnemius muscle[24], that was not restored after treatment. The capability of AAV vector to efficiently transduce satellite cells is controversial with studies supporting

absence of transduction[30] or efficient transduction using serotypes 8 and 9 or even with serotype 1 despite a lower efficacy.[31] Therefore, the absence of *Pax7* rescue might result from limited transduction of satellite cells with AAV1 vector that may be improved in the future by other serotypes. Nevertheless, our results show that the correction of *Pax7* expression is not a prerequisite to prevent fiber atrophy.

Our study identified a 2-fold increase in DNM2 protein content in heterozygous Tibialis anterior muscle from 6-month-old mice, not seen at mRNA level suggesting that this post-transcriptional regulation results from mutant protein accumulation/absence of degradation. Of note, an increase in DNM2 protein without increase in mRNA expression has been also reported in XLCNM disease.[19] DNM2 protein accumulation was not observed at younger age in this KI-*Dnm2*^{R465W} model (in neonates and 2-month-old mice)[23,26], while intracellular accumulations have been already observed by immunofluorescence in isolated HTZ muscle fiber.[23] However, in the recent model of severe CNM KI-*Dnm2*$^{S619L/+}$, a 2-fold increase in DNM2 protein level was also demonstrated at 2 months of age[32]. In accordance with these observations, transgenic zebrafish models expressing the R465W and S619L mutants showed a protein mislocalization and aggregation that correlate with the severity of the CNM mutations.[33] Finally, the propensity of several DNM2 mutants to form abnormally stable oligomers compare to WT has been already reported *in vitro*.[32] Autophagy and the ubiquitin–proteasome system are the two major intracellular quality control and recycling mechanisms that are responsible for degradation of misfolded or aggregated proteins.[34] Interestingly, autophagy was shown to be directly impacted by *Dnm2* mutation.[35,36] Therefore, the DNM2 oligomers/polymers formed by the DNM2 R465W mutant could be initially efficiently handle by intracellular quality control system, who would become overloaded and/or mis-functional with time leading to the increase in DNM2 protein level. However, we confirmed that the abnormal activation of the ubiquitin-proteasome and autophagy genes observed at 2 months of age in heterozygous mice that normalizes at 8

months[23] remains normalized at 13 months. The decrease in Murf1 and Gabarapl1 expression observed in treated heterozygous mice could be due to a direct regulation of these genes by DNM2.

Altogether, the propensity to aggregate shared by several *Dnm2* CNM mutation (and not seen in CMT-related mutation[33]), the correlation between the degree of aggregation and the severity of the disease[32] and this study, and our observation of increase with age in parallel of the disease progression, argue in favor of their contribution to pathogenesis. Along the same lines, it is noteworthy that overexpression of WT DNM2 by itself could trigger muscle defects[37,38] underlying the importance of a tiny DNM2 level regulation for proper muscle development, maturation, and maintenance.

Our study also led to identify a physiological decrease of DNM2 protein content in healthy muscle with age and this age-related decrease seems to be muscle-specific. Our results argue for the relevance of this DNM2 decrease with age in human muscle from healthy controls, while the level of DNM2 expression in CNM patients remains in the range of young controls regardless of their age. In the literature, few studies have investigated the localization or the level of DNM2 in patients. Normal expression of Dynamin 2 mRNA and protein has been reported in fibroblasts from CNM patients.[39–41] In addition, aggregates have been reported in one late-onset patient with a normal protein amount[9] and recently abnormal western blot profile was reported for a severe young CNM patient.[32] Altogether these data may suggest that the level of DNM2 required for proper muscle function would vary according to muscle maturation stage and this process would be impaired more or less early according to the *DNM2* mutation, leading to unbalanced WT/mutant protein ratio with age and reinforcing under this postulate the asset of a mutant specific approach.

AAVs transgene expression results from a complex multistep process including AAV entry by endocytosis, microtubule-dependent endosomal trafficking, endosome escape, nuclear

import, capsid uncoating allowing single-strand DNA release and double strand conversion.[42] Given the known functions of DNM2, several steps of AAV processing could be additively affected by DNM2 dysfunction. Our study shows an AAV transduction defect in the KI-*Dnm2*$^{R465W/+}$ model which is probably already present in young mice. Indeed, the amount of viral genome detected after one year in mice injected at one month of age is lower in HTZ than in WT mice, while this amount is comparable after one month. This argues for a higher rate of viral genome loss with time in HTZ muscles that would be independent of regeneration. However, the benefit on contractile properties despite undetectable silencing of the mutated allele in 6-month-old mice supports a low therapeutic threshold and is encouraging to persevere in the improvement of AAV-transduction in our model. Notably, insulin treatment[43], removal of capsid phosphorylation sites[44] or stimulation of autophagy[45] have been reported to improve transduction efficiency. Otherwise, other serotypes or non-viral delivery can be considered alone or in combination with AAV treatment. In the latter case the non-viral delivery could transiently improve the muscle state in order to enhance the transduction capabilities at the time of AAV injection.

To date there is no curative treatment available for AD-CNM patients, despite a treatment with acetylcholinesterase inhibitor reported to improve muscle strength in few DNM2-CNM patients.[46] We have previously succeeded to correct the *DNM2* mRNA by trans-splicing, but with a low efficiency.[47] Non-allele specific *Dnm2* RNAi (*i.e.* targeting both alleles of *Dnm2)* mediated by antisense oligonucleotides was also reported to efficiently improve the progression of the disease in two AD-CNM mouse models (i.e. KI-*Dnm2*$^{R465W/+}$ and KI-*Dnm2*$^{S619L/+}$).[26,32] Unfortunately, the long-term benefits have not been reported using this approach. The proof-of-concept of AS-RNAi therapy *in vitro* and *in vivo*[22] and our current demonstration of long-term efficacy in an animal model enlarge the therapeutic possibilities for the disease. In addition to efficiency and specificity provided by RNAi, AS-RNAi introduces a third property of safety

since 50% expression is preserved from the healthy untargeted allele. This may be of particular importance in a context of physiological decrease with age of the DNM2 expression.

In conclusion, the demonstration that time does not impair the treatment benefit nor the level of mutant silencing associated with the prevention of protein accumulation and absence of toxicity confirms allele-specific RNA interference mediated by AAV delivery as a strategy of choice to treat autosomal dominant centronuclear myopathy due to Dynamin 2 mutations.

Materials and Methods

Data Analysis and Statistics

Graphics and statistical analyses were performed with GraphPad Prism software version 9. Values were expressed as means ± SEM. The number of samples (n), representing the number of independent biological replicates, was indicated in the figure legends. For molecular analysis the experiments were repeated at least three times per biological replicate and averaged. We used nonparametric statistical tests to analyze our data since the normality could not be assume or tested or the variance were not equal between groups. Statistical comparisons between two groups were performed using unpaired two-tailed Mann-Whitney *U*-test as specified. Spearman correlation analysis was used to evaluate the strength of relationship between DNM2 protein content and age. Statistical tests applied are indicated in the figure legends. P values < 0.05 were considered as statistically significant. In most of the figures, the gels are cropped for more conciseness but samples presented were run on a same gel.

Total RNA extraction and cDNA analysis

Total RNAs were isolated from muscle by TRIZOL reagent (Life Technologies, France) following standard protocol after disruption using Fastprep Lysing Matrix D and Fastprep apparatus (MP Biomedical, France). Total RNA (1 µg) were submitted to reverse transcription using the Superscript III reverse transcriptase kit (Life Technologies) and oligo-dT primers. The cDNAs were amplified by PCR under the following conditions: 96°C for 5 min, cycles of 30 s at 96°C, 30 s at the appropriate temperature (58 to 62°C), 30 s at 72°C, and a final step of 7 min at 72°C. Semi-quantitative RT-PCR was used to determine the total *Dnm2* expression, the appropriate number of PCR cycles has been selected in order to have the amplification in the exponential range (i.e. 23 cycles to amplify *Gapdh* and 28 cycles for *Dnm2*). Sequences of the primers were indicated previously [22]. To quantify allele-specific silencing, an assay was developed using EcoNI restriction enzyme allowing discrimination between wild-type and

mutant cDNAs. *Dnm2* PCR products (393 base-pair) containing the mutation was EcoNI digested and run on agarose gel. EcoNI digests only RT-PCR product amplified from the WT leading to 2 fragments (247 and 146 base-pair) allowing discrimination between WT and mutated alleles. The densitometric ratio between the non-digested band (mutated) and the sum of the signal for the two digested bands (wild-type) is done and compared with untreated conditions where this ratio is set to 1 to estimate the efficiency of the siRNA on the mutated allele. The digestion of murine *Dnm2* amplicons was performed after 32 cycles at the end of the exponential phase of amplification. For this assay, the half of the PCR products was digested using 2U of EcoNI (New England Biolabs, France) for 2 h at 37°C. Image acquisition of PCR products after agarose gel electrophoresis was performed using a Geni2 gel imaging system (Ozyme, France) and associated-signal was quantified using ImageJ Software (NIH; http://rsbweb.nih.gov/ij).

Semi-quantitative RT-PCR was also used to determine the total expression of two interferon-induced genes (*Oas1* and *Stat1*) with appropriate number of PCR cycles selected in order to have the amplification in the exponential range *(i.e.* 34 cycles to amplify *OasI*, 36 cycles to amplify *Stat1*). Sequences of the primers were indicated previously.[22] *Pax7*, *Gabarapl1, p62 Atg4*, *Murf1 and Atrogin 1* mRNA quantification was performed by real-time PCR using a Lightcycler 480 II (Roche, Switzerland) and 1X SYBR Green (Roche, Switzerland) reactions using 0.5 µM of forward and reverse primers, and 5 µL of cDNA diluted at 1:10 in nuclease-free water. PCR cycles were a 5 min 95°C pre-incubation step followed by 45 cycles with a 95°C denaturation for 10 s, 58°C or 60°C annealing for 15 s and 72°C extension for 15 s. Relative expression was calculated as mean values of $2^{-\Delta\Delta CT}$ normalized using the *Atpase* housekeeping gene. Primers sequences are *Pax7* Fw-GAG TTC GAT TAG CCG AGT GC, Rv-GTG TTT GGC TTT CTT CTC GC, *Atpase* Fw-CCCCCTGTTCAGGTCTACGG, Rv-GACGGTGCGCTTGATGTAGG, *Atrogin1* Fw -GCCTTCAAAGGCCTCACG and Rv -

CTGAGCACATGCAGGTCTGGG, *Murf1* Fw -CGACCGAGTGCAGACGATCATCTC and Rv-GTGTCAAACTTCTGACTCAGC, *Gabarap11* Fw-CATCGTGGAGAAGGCTCCTA and Fw-ATACAGCTGGCCCATGGTAG, *P62*, *Atg4* Fw-ACAGATGATCTTTGCCCAGG and Rv-TAGACTTGCCTTCGCCAACT, P62 Fw- GCTCAGGAGGAGACGATGAC and Rv-AGGGGTCTAGAGAGCTTGGC.

Protein extraction and western blot

Frozen TA muscles and tissues were mechanically grinding in liquid nitrogen using a ceramic mortar and pestle precooled in dry ice. Powder was then weighed and homogenized in cold lysis buffer (200 µl per 30 mg of powder) containing 50 mM of Tris-HCl pH 7.5, 150 mM NaCl, 1 mM EDTA, NP40 1% supplemented with protease inhibitor cocktail 1% (Sigma-Aldrich, France). Samples was then incubated under agitation in cold-room for 4 hours and sonicated on ice. After centrifugation (14,000 g, 4°C, 15 min), protein concentration in the supernatant was determined with the BCA Protein Assay Kit (Thermo Scientific Pierce, France). Ten µg of proteins were mixed with loading buffer (50 mM Tris–HCl, SDS 2%, glycerol 10%, 2-mercaptoethanol 1% and bromophenol blue) and denaturated at 90°C for 5 min. For TA, protein extracts samples were separated on SDS–PAGE 10% and transferred onto PVDF membranes (0.45 µm pore size, Life Technologies) overnight at 100 mA at 4°C. The other protein extracts (*i.e.* mouse tissues and human muscles) were separated on 10% Mini-PROTEAN® TGX Stain-Free (Bio-Rad) and the gel was transferred on nitrocellulose membrane using Transblot Turbo RTA transfer kit for 8 minutes at 2.5A. Total protein loading was determined by stain free staining. After transfer, membranes were blocked for 1 h at room temperature in PBS containing non-fat dry milk 5% and Tween-20 0.1% and then exposed to rabbit polyclonal anti-Dynamin 2 antibody (Abcam ab3457, dilution 1:1000 or ab65556 dilution 1:4000, United Kingdom) or rabbit polyclonal anti-GAPDH antibody (Sc-25778 dilution 1:2000, Santa Cruz, France) in PBS-Tween-20 0.1%, milk 1% overnight at 4°C.

Membranes were rinsed in PBS-Tween-20 0.1% and incubated 1h at room temperature with horseradish peroxidase-conjugated secondary antibody (anti-rabbit from Jackson ImmunoResearch, United Kingdom) in PBS-Tween-20 0.1%. Chemiluminescence was detected using ECL detection Kit (Merck-Millipore, Germany) in a Chemidoc Imaging Systems (Biorad, France) and signal quantification was performed using ImageJ software.

AAV production

A cassette containing the small hairpin (sh) RNA under the control of H1 RNA polymerase III promoter has been inserted in a pSMD2 expression plasmid. The small-hairpin (sh)-9 RNA was generated from the *Dnm2* 19 nucleotides siRNA targeting the mouse mutation (c.1393 A>T, p.R465W) and harboring a mismatch with the wild type sequence in position 9 of the sense strand. This siRNA has been previously selected for its efficacy and allele specificity.[22] The shRNA maker function of the Serial Cloner software was used to generate shRNA sequences (available on request) for subsequent subcloning in the pH1-Super plasmid. Sense and antisense sh9-RNA (Eurogentec, Belgium) was annealed using annealing solution (pSilencer kit, Ambion) according to manufacturer's instructions and inserted in BglII - HindIII sites in pH1-Super plasmid. The cassette pH1-sh9RNA was then inserted in the pSMD2 between BamH1 and SalI sites. AAV vectors (serotype 1) were produced in HEK293 cells after transfection of the pSMD2-shRNA plasmid or empty pSMD2 plasmid, the pXX6 plasmid coding for viral helper genes required for AAV production and the pRepCap plasmid (p0001) coding for AAV1 capsid as described previously. Viral particles were purified on iodixanol gradients and concentrated on Amicon Ultra-15 100K columns (Merck-Millipore). The concentration of viral genomes (vg/ml) was determined by quantitative real-time PCR on a LightCycler480 (Roche diagnostic, France) by using TaqMan probe in the inverted terminal repeat (ITR) sequences. A control pSMD2 plasmid was tenfold serially diluted (from 10^7 to 10^1 copies) and used as a control to establish the standard curve for absolute quantification.

Sequences of primers and probes are available on request or indicated previously.[22] Adeno-associated virus (AAV) serotype 1 vectors containing shRNA specific of the mutant allele (AAV-sh9) and a control (AAV-control) were produced.

Mice and in vivo transduction

The dynamin 2 mutant mouse line was established on C57Bl/6 background at the Mouse Clinical Institute (MCI, Illkirch, France; http:// www-mci.u-strasbg.fr)[23]. All mice used in this study were housed on a 12-h light/dark cycle and received standard diet and water ad libitum in the animal facility of Sorbonne University (Paris, France). Male heterozygous KI-*Dnm2*^{R465W} mice were injected at 1 and 6 months of age under isoflurane anesthesia. We chose male mice since the characterization of the model has been done on male, the WT littermates were used as controls. Two intramuscular injections of 30 µl within 24h interval were performed using 29G needle in TA muscles. AAV-sh9 and AAV-control were injected at 1 month of age and at 6 months of age in order to achieve 10^{11} and 10^{12} vg/muscle respectively. Age-matched WT mice non-injected or injected with the AAV-control or PBS were used as control.

For 1-month old mice injected for 1 year, 23 heterozygous mice have been injected (*i.e.* 23 right TA with the AAV1-sh9 and 23 left TA with the AAV1-control) and 11 wild-type mice (*i.e.* 11 right TA with the AAV1-control and 11 left TA with PBS), all of them were analyzed for the muscle force. We decided to inject a high number of mice to prevent potential lost due to death of mice considering the long period. Eleven heterozygous TA of each conditions and 14 wild-type TA were then used for molecular biology, 9 heterozygous TA of each condition and 8 wild-type were used for histology. For 6-month old mice injected for 3 months with high dose of AAV1-sh9, 5 heterozygous mice have been injected (*i.e.* 4 TA with the AAV1-sh9 and 6 TA with the PBS) and 11 wild-type mice (*i.e.* 11 TA with PBS), all of them were analyzed for the muscle force, molecular biology and histology.

Muscle contractile properties

The isometric contractile properties of TA muscles were studied *in situ* on mice anesthetized with 60 mg/kg pentobarbital. The distal tendon of the TA muscle was attached to a lever arm of a servomotor system (305B Dual-Mode Lever, Aurora Scientific). The sciatic nerve was stimulated by a bipolar silver electrode using a supramaximal (10 V) square wave pulse of 0.1 ms duration. Absolute maximal isometric tetanic force was measured during isometric contractions in response to electrical stimulation (frequency of 25–150 Hz; train of stimulation of 500 ms). All isometric contraction measurements were made at optimal muscle length. Force are expressed in grams (1 gram = 9.8 mNewton). Mice were sacrificed by cervical dislocation and TA muscles were weighted. Specific maximal force was calculated by dividing absolute force by muscle weight.

Histomorphological analyses

TA muscles were frozen in liquid nitrogen-cooled isopentane. Transverse sections of TA muscle (8 µm thick) were stained with hematoxylin and eosin (HE), Succinate Dehydrogenase staining (SDH) and reduced diphosphopyridine nucleotide diaphorase staining (DPNH) by standard methods. Light microscopy was performed using an Axioscope Z1 Slide scanners (Zeiss, France) at 20X magnification. Exposure settings were identical between compared samples and viewed at room temperature. Histomorphological abnormalities were manually counted on SDH staining using cell counter plugin Fiji software[48], 8 untreated and 8 treated heterozygous Tibialis anterior sections from different animals were counted

Immunocytochemistry

For immunocytochemistry, muscle cryosections (8 µm thick) were fixed in paraformaldehyde 4% (15 min at room temperature). After washing in PBS, cryosections were permeabilized in Triton X-100 0.5% in PBS for 10 min at room temperature and blocked in PBS-Triton X-100 0.1%, BSA 5% and Donkey serum 5% for 30 min. Samples were incubated with rabbit anti-Laminin (Abcam ab11575) overnight at 4°C, in PBS with Triton X-100 0.1% and BSA 1%.

After PBS-Triton X-100 0.1% washes, samples were incubated with Goat anti-rabbit AlexaFluor568 secondary antibody (Life Technologies, France) for 60 min at room temperature. For satellite cell staining, transverse 8 µm-cross-sections were fixed with 4% paraformaldehyde, blocked in PBS containing 5% FCS and 0.01% triton-X100, and then incubated overnight with primary antibody against PAX7 (1:20; DSHB, US) and labelled with AlexaFluor 568 (1:300, Life Technologies, France). Slides were then stained with 4',6-diamidino-2-phenylindole (DAPI) for nuclei staining. The slides were mounted with Vectashield mounting medium (Vector Laboratories, United Kingdom). Fluorescent images acquisition was performed at 20X magnification on Axioscope Z1 Slide scanners (Zeiss, France) for Laminin and on a Nikon Ti2 microscope, driven by Metamorph Software (Roper), equipped with a motorized stage and a Yokogawa CSU-W1 spinning disk head coupled with a Prime 95 sCMOS camera (Photometrics) for PAX7. For quantification of fibre size, images of TA muscle sections labelled with anti-laminin antibody were used to automatically determine the Feret diameter of each fibre after manual segmentation using the Fiji software. The normal distribution of the values was plotted using Microsoft Excel software (8 heterozygous untreated, 8 heterozygous treated and 6 wild-type Tibialis anterior sections from different animals were analyzed). Satellite cells were counted using the "cell counter" plugin of ImageJ. Tibialis from each condition (WT (n=6), untreated heterozygous (n=5) and treated heterozygous (n=5) were imaged at 20 X magnification and at least 5 different fields were analyzed (corresponding to an average of 900 fibers).

Viral genome quantification

Viral infection efficacy was evaluated through quantification of viral genomes in injected muscles. Genomic DNA was extracted from mouse muscle sections using DNA purification kit (Promega, France) according to the manufacturer’s protocol. Copy numbers of AAV genomes were quantified on 100 ng of genomic DNA by quantitative real-time PCR on a LightCycler480

(Roche diagnostic, France) by using TaqMan probe. A linearized plasmid containing ITR sequences was used to establish the standard curve for absolute quantification. Sequences of primers also used for viral titration are available on request.

Human biopsies

Twelve control human muscle samples from patients ranging from ages 3 to 60 years old were obtained from the MyoBank-AFM bank of tissues for research, a partner in the EU network EuroBioBank, or from the Morphological Unit of the Institute of Myology (Paris, France) in accordance with European recommendations and French legislation. The five CNM-patient's biopsies were obtained from the Morphological unit, and are ranging from age 1 month to 48 years and harbor different DNM2 missense mutations (*i.e*. the DNM2 E611K, R369W, A618T, R465W and R522H).

Study approval

Animal studies conform to the French laws and regulations concerning the use of animals for research and were approved by an external Ethical committee (APAFIS#21085-2019060719395546) delivered by the French Ministry of Higher Education and Scientific Research).

Acknowledgments

We thank the Histomics Platform from the Brain and Spinal cord Institute (Paris, France) for light microscopy imaging, the MyoBank-AFM and the Histopathology Laboratory from the Institut de Myologie (Paris, France) for providing human muscles samples, the Penn Vector Core, Gene Therapy Program (University of Pennsylvania, Philadelphia, USA) for providing pAAV1 plasmid (p0001). We would like to thank Catherine Coirault for fruitful discussions and comments. This work was supported by the Institut National de la Santé et de la Recherche Médicale (INSERM), INSERM transfert (CoPoC grant), the Association Institut de Myologie

(AIM), Sorbonne Université, and the Agence Nationale de la Recherche ANR Dynather (ANR-18-CE17-0006-02 to MBi).

Author contributions

DT and MBi conceived and designed the experiments. DT, BP, LM, ML, MBe, and MBi performed the experiments. LJ and SBZ produced the AAV vector. MTB and NR provided the human muscle samples and helpful discussions. DT, LM and MBi analysed the data. DT and MBi wrote the manuscript.

Conflict of interest statement: The authors have declared that no conflict of interest exists.

Key words: allele-specific silencing; gene therapy; dominant centronuclear myopathy; Dynamin 2; RNA interference, in vivo long-term benefits

Bibliography

1. Romero, N.B. (2010). Centronuclear myopathies: A widening concept. Neuromuscul. Disord. *20*, 223–228.
2. Böhm, J., Biancalana, V., DeChene, E.T., Bitoun, M., Pierson, C.R., Schaefer, E., Karasoy, H., Dempsey, M.A., Klein, F., Dondaine, N., et al. (2012). Mutation spectrum in the large gtpase dynamin 2, and genotype-phenotype correlation in autosomal dominant centronuclear myopathy. Hum. Mutat. *33*, 949–959.
3. Bitoun, M., Maugenre, S., Jeannet, P.Y., Lacène, E., Ferrer, X., Laforêt, P., Martin, J.J., Laporte, J., Lochmüller, H., Beggs, A.H., et al. (2005). Mutations in dynamin 2 cause dominant centronuclear myopathy. Nat. Genet. *37*, 1207–1209.
4. Biancalana, V., Romero, N.B., Thuestad, I.J., Ignatius, J., Kataja, J., Gardberg, M., Héron, D., Malfatti, E., Oldfors, A., and Laporte, J. (2018). Some DNM2 mutations cause extremely severe congenital myopathy and phenocopy myotubular myopathy. Acta Neuropathol. Commun. *6*, 93.
5. Casar-Borota, O., Jacobsson, J., Libelius, R., Oldfors, C.H., Malfatti, E., Romero, N.B., and Oldfors, A. (2015). A novel dynamin-2 gene mutation associated with a late-onset centronuclear myopathy with necklace fibres. Neuromuscul. Disord. *25*, 345–348.
6. Catteruccia, M., Fattori, F., Codemo, V., Ruggiero, L., Maggi, L., Tasca, G., Fiorillo, C., Pane, M., Berardinelli, A., Verardo, M., et al. (2013). Centronuclear myopathy related to dynamin 2 mutations: Clinical, morphological, muscle imaging and genetic features of an Italian cohort. Neuromuscul. Disord. *23*, 229–238.
7. Chen, T., Pu, C., Wang, Q., Liu, J., Mao, Y., and Shi, Q. (2015). Clinical, pathological, and genetic features of dynamin-2-related centronuclear myopathy in China. Neurol. Sci. *36*, 735–741.
8. Fujise, K., Okubo, M., Abe, T., Yamada, H., Takei, K., Nishino, I., Takeda, T., and Noguchi, S. (2022). Imaging-based evaluation of pathogenicity by novel DNM2 variants associated with centronuclear myopathy. Hum. Mutat. *43*, 169–179.
9. Kierdaszuk, B., Berdynski, M., Karolczak, J., Redowicz, M.J., Zekanowski, C., and Kaminska, A.M. (2013). A novel mutation in the DNM2 gene impairs dynamin 2 localization in skeletal muscle of a patient with late onset centronuclear myopathy. Neuromuscul. Disord. *23*, 219–228.
10. Neto, O.A., De Martins, C.A., Carvalho, M., Chadi, G., Seitz, K.W., Oliveira, A.S.B., Conti Reed, U., Laporte, J., and Zanoteli, E. (2015). DNM2 mutations in a cohort of sporadic patients with centronuclear myopathy. Genet. Mol. Biol. *38*, 147–151.
11. Reumers, S.F.I., Erasmus, C.E., Bouman, K., Pennings, M., Schouten, M., Kusters, B., Duijkers, F.A.M., van der Kooi, A., Jaeger, B., Verschuuren-Bemelmans, C.C., et al. (2021). Clinical, genetic, and histological features of centronuclear myopathy in the Netherlands. Clin. Genet. *100*, 692–702.
12. Züchner, S., Noureddine, M., Kennerson, M., Verhoeven, K., Claeys, K., De Jonghe, P., Merory, J., Oliveira, S.A., Speer, M.C., Stenger, J.E., et al. (2005). Mutations in the pleckstrin homology domain of dynamin 2 cause dominant intermediate Charcot-Marie-Tooth disease. Nat. Genet. *37*, 289–294.
13. Sambuughin, N., Goldfarb, L.G., Sivtseva, T.M., Davydova, T.K., Vladimirtsev, V.A., Osakovskiy, V.L., Danilova, A.P., Nikitina, R.S., Ylakhova, A.N., Diachkovskaya, M.P., et al. (2015). Adult-onset autosomal dominant spastic paraplegia linked to a GTPase-effector domain mutation of dynamin 2. BMC Neurol. *15*, 223.
14. Antonny, B., Burd, C., De Camilli, P., Chen, E., Daumke, O., Faelber, K., Ford, M., Frolov, V.A., Frost, A., Hinshaw, J.E., et al. (2016). Membrane fission by dynamin: what

we know and what we need to know. EMBO J. *35*, 2270–2284.

15. Ferguson, S.M., and De Camilli, P. (2012). Dynamin, a membrane-remodelling GTPase. Nat. Rev. Mol. Cell Biol. *13*, 75–88.

16. Durieux, A.C., Prudhon, B., Guicheney, P., and Bitoun, M. (2010). Dynamin 2 and human diseases. J. Mol. Med. *88*, 339–350.

17. Kenniston, J.A., and Lemmon, M.A. (2010). Dynamin GTPase regulation is altered by PH domain mutations found in centronuclear myopathy patients. EMBO J. *29*, 3054–3067.

18. Wang, L., Barylko, B., Byers, C., Ross, J.A., Jameson, D.M., and Albanesi, J.P. (2010). Dynamin 2 mutants linked to centronuclear myopathies form abnormally stable polymers. J. Biol. Chem. *285*, 22753–22757.

19. Cowling, B.S., Chevremont, T., Prokic, I., Kretz, C., Ferry, A., Coirault, C., Koutsopoulos, O., Laugel, V., Romero, N.B., and Laporte, J. (2014). Reducing dynamin 2 expression rescues X-linked centronuclear myopathy. J. Clin. Invest. *124*, 1350–1363.

20. Ferguson, S., Raimondi, A., Paradise, S., Shen, H., Mesaki, K., Ferguson, A., Destaing, O., Ko, G., Takasaki, J., Cremona, O., et al. (2009). Coordinated Actions of Actin and BAR Proteins Upstream of Dynamin at Endocytic Clathrin-Coated Pits. Dev. Cell *17*, 811–822.

21. Trochet, D., Prudhon, B., Vassilopoulos, S., and Bitoun, M. (2015). Therapy for Dominant Inherited Diseases by Allele-Specific RNA Interference: Successes and Pitfalls. Curr. Gene Ther. *15*, 503–510.

22. Trochet, D., Prudhon, B., Beuvin, M., Peccate, C., Lorain, S., Julien, L., Benkhelifa-Ziyyat, S., Rabai, A., Mamchaoui, K., Ferry, A., et al. (2018). Allele-specific silencing therapy for Dynamin 2-related dominant centronuclear myopathy. EMBO Mol. Med. *10*, 239–253.

23. Durieux, A.C., Vignaud, A., Prudhon, B., Viou, M.T., Beuvin, M., Vassilopoulos, S., Fraysse, B., Ferry, A., Lainé, J., Romero, N.B., et al. (2010). A centronuclear myopathy-dynamin 2 mutation impairs skeletal muscle structure and function in mice. Hum. Mol. Genet. *19*, 4820–4836.

24. F. Almeida, C., Bitoun, M., and Vainzof, M. (2021). Satellite cells deficiency and defective regeneration in dynamin 2-related centronuclear myopathy. FASEB J. *35*, 1–14.

25. Fongy, A., Falcone, S., Lainé, J., Prudhon, B., Martins-Bach, A., and Bitoun, M. (2019). Nuclear defects in skeletal muscle from a Dynamin 2-linked centronuclear myopathy mouse model. Sci. Rep. *9*, 1580.

26. Buono, S., Ross, J.A., Tasfaout, H., Levy, Y., Kretz, C., Tayefeh, L., Matson, J., Guo, S., Kessler, P., Monia, B.P., et al. (2018). Reducing dynamin 2 (DNM2) rescues DNM2-related dominant centronuclear myopathy. Proc. Natl. Acad. Sci. U. S. A. *115*, 11066–11071.

27. Buchlis, G., Podsakoff, G.M., Radu, A., Hawk, S.M., Flake, A.W., Mingozzi, F., and High, K.A. (2012). Factor IX expression in skeletal muscle of a severe hemophilia B patient 10 years after AAV-mediated gene transfer. Blood *119*, 3038–3041.

28. Bish, L.T., Morine, K., Sleeper, M.M., Sanmiguel, J., Wu, D., Gao, G., Wilson, J.M., and Sweeney, H.L. (2008). Adeno-associated virus (AAV) serotype 9 provides global cardiac gene transfer superior to AAV1, AAV6, AAV7, and AAV8 in the mouse and rat. Hum. Gene Ther. *19*, 1359–1368.

29. Jiang, J., Wakimoto, H., Seidman, J.G., and Seidman, C.E. (2013). Allele-specific silencing of mutant Myh6 transcripts in mice suppresses hypertrophic cardiomyopathy. Science (80-.). *342*, 111–114.

30. Arnett, A.L., Konieczny, P., Ramos, J.N., Hall, J., Odom, G., Yablonka-Reuveni, Z.,

Chamberlain, J.R., and Chamberlain, J.S. (2014). Adeno-associated viral vectors do not efficiently target muscle satellite cells. Mol. Ther. - Methods Clin. Dev. *1*, 14038.

31. Kwon, J.B., Ettyreddy, A.R., Vankara, A., Bohning, J.D., Devlin, G., Hauschka, S.D., Asokan, A., and Gersbach, C.A. (2020). In Vivo Gene Editing of Muscle Stem Cells with Adeno-Associated Viral Vectors in a Mouse Model of Duchenne Muscular Dystrophy. Mol. Ther. - Methods Clin. Dev. *19*, 320–329.

32. Muñoz, X.M., Kretz, C., Silva-Rojas, R., Ochala, J., Menuet, A., Romero, N.B., Cowling, B.S., and Laporte, J. (2020). Physiological impact and disease reversion for the severe form of centronuclear myopathy linked to dynamin. JCI Insight *5*, e137899.

33. Zhao, M., Smith, L., Volpatti, J., Fabian, L., and Dowling, J.J. (2019). Insights into wild-type dynamin 2 and the consequences of DNM2 mutations from transgenic zebrafish. Hum. Mol. Genet. *28*, 4186–4196.

34. Kocaturk, N.M., and Gozuacik, D. (2018). Crosstalk between mammalian autophagy and the ubiquitin-proteasome system. Front. Cell Dev. Biol. *6*.

35. Durieux, A.C., Vassilopoulos, S., Lainé, J., Fraysse, B., Briñas, L., Prudhon, B., Castells, J., Freyssenet, D., Bonne, G., Guicheney, P., et al. (2012). A Centronuclear Myopathy - Dynamin 2 Mutation Impairs Autophagy in Mice. Traffic *13*, 869–879.

36. Puri, C., Manni, M.M., Vicinanza, M., Hilcenko, C., Zhu, Y., Runwal, G., Stamatakou, E., Menzies, F.M., Mamchaoui, K., Bitoun, M., et al. (2020). A DNM2 Centronuclear Myopathy Mutation Reveals a Link between Recycling Endosome Scission and Autophagy. Dev. Cell *53*, 154-168.e6.

37. Cowling, B.S., Toussaint, A., Amoasii, L., Koebel, P., Ferry, A., Davignon, L., Nishino, I., Mandel, J.L., and Laporte, J. (2011). Increased expression of wild-type or a centronuclear myopathy mutant of dynamin 2 in skeletal muscle of adult mice leads to structural defects and muscle weakness. Am. J. Pathol. *178*, 2224–2235.

38. Liu, N., Bezprozvannaya, S., Shelton, J.M., Frisard, M.I., Hulver, M.W., McMillan, R.P., Wu, Y., Voelker, K.A., Grange, R.W., Richardson, J.A., et al. (2011). Mice lacking microRNA 133a develop dynamin 2-dependent centronuclear myopathy. J. Clin. Invest. *121*, 3258–3268.

39. Bitoun, M., Durieux, A.C. cile, Prudhon, B., Bevilacqua, J.A., Herledan, A., Sakanyan, V., Urtizberea, A., Cartier, L., Romero, N.B., and Guicheney, P. (2009). Dynamin 2 mutations associated with human diseases impair clathrin-mediated receptor endocytosis. Hum. Mutat. *30*, 1419–1427.

40. Echaniz-Laguna, A., Nicot, A.S., Carré, S., Franques, J., Tranchant, C., Dondaine, N., Biancalana, V., Mandel, J.L., and Laporte, J. (2007). Subtle central and peripheral nervous system abnormalities in a family with centronuclear myopathy and a novel dynamin 2 gene mutation. Neuromuscul. Disord. *17*, 955–959.

41. Koutsopoulos, O.S., Kretz, C., Weller, C.M., Roux, A., Mojzisova, H., Böhm, J., Koch, C., Toussaint, A., Heckel, E., Stemkens, D., et al. (2013). Dynamin 2 homozygous mutation in humans with a lethal congenital syndrome. Eur. J. Hum. Genet. *21*, 637–642.

42. Nonnenmacher, M., and Weber, T. (2012). Intracellular transport of recombinant adeno-associated virus vectors. Gene Ther. *19*, 649–658.

43. Carrig, S., Bijjiga, E., Wopat, M.J., and Martino, A.T. (2016). Insulin Therapy Improves Adeno-Associated Virus Transduction of Liver and Skeletal Muscle in Mice and Cultured Cells. *27*, 892–906.

44. Qiao, C., Zhang, W., Yuan, Z., Shin, J.-H., Li, J., Jayandharan, G.R., Zhong, L., Srivastava, A., Xiao, X., and Duan, D. (2010). Adeno-Associated Virus Serotype 6 Capsid Tyrosine-to-Phenylalanine Mutations Improve Gene Transfer to Skeletal Muscle. Hum. Gene Ther. *21*, 1343–1348.

45. Hösel, M., Huber, A., Bohlen, S., Lucifora, J., Ronzitti, G., Puzzo, F., Boisgerault, F.,

Hacker, U.T., Kwanten, W.J., Klöting, N., et al. (2017). Autophagy determines efficiency of liver-directed gene therapy with adeno-associated viral vectors. Hepatology *66*, 252–265.

46. Gibbs, E.M., Clarke, N.F., Rose, K., Oates, E.C., Webster, R., Feldman, E.L., and Dowling, J.J. (2013). Neuromuscular junction abnormalities in DNM2-related centronuclear myopathy. J. Mol. Med. *91*, 727–737.

47. Trochet, D., Prudhon, B., Jollet, A., Lorain, S., and Bitoun, M. (2016). Reprogramming the Dynamin 2 mRNA by Spliceosome-mediated RNA Trans-splicing. Mol. Ther. - Nucleic Acids *5*, e362.

48. Schindelin, J., Arganda-Carreras, I., Frise, E., Kaynig, V., Longair, M., Pietzsch, T., Preibisch, S., Rueden, C., Saalfeld, S., Schmid, B., et al. (2012). Fiji: An open-source platform for biological-image analysis. Nat. Methods *9*, 676–682.

Figures and legends

Figure 1: Muscle phenotypic rescue persists at least one year long. A. Muscle mass relative to body weight in milligrams/grams from WT and AAV-shRNA-injected mice (HTZ n=23, WT n = 22). **B**. Histogram of the mean Feret diameter (WT n=6, HTZ n=8). **C.** Combined frequencies of fibre size in TA muscles (WT n=6, HTZ n =8 of each conditions). **D.** Histochemical staining of TA sections from WT and AAV-injected HTZ mice. HE: haematoxylin–eosin staining. SDH: Succinate Dehydrogenase staining. Asterisks indicate fibers with abnormal central accumulations. Scale bars = 50 µm. **E**. Quantification of histological abnormality. Scatter plot represents individual percentages of histological abnormality from heterozygous control or treated mice (HTZ-ctl n = 6, HTZ treated n = 4). **F**. Relative *Pax7* mRNA expression in WT, HTZ control and HTZ muscles injected with AAV-sh9. WT was used as the normalizer sample (WT n= 11, HTZ n = 11). **G**. Absolute maximal force (g: grams) **H**. Specific maximal force developed by TA muscles (In G and H HTZ n = 23, WT n = 22). Data information: In scatters blot (A, B, E–H), bars represent mean ± SEM. Statistical analysis was performed using a two-tailed Mann–Whitney U-test. *P < 0.05, **P < 0.01 and ***P < 0.001 compared to WT.

Figure 2: Viral amount and expression of interferon-induced genes in AAV-injected mice
A. Quantification of the viral genomes (vg) per ng of genomic DNA in mice injected with AAV-sh9 or control. WT muscles injected with PBS were included as negative control (HTZ n = 11, WT-control n=6, WT-PBS n=5). **B**. Quantification of expression of the interferon-induced genes *Oas1* and *Stat1* mRNA relative to *Gapdh* mRNA by RT–PCR in muscle from 13-month-old mice treated at 1 month of age. Left panel: *Oas1* expression. Right panel: *Stat1* expression. (HTZ-control n = 11, HTZ-control n=11, WT-PBS n=11). Data information: Scatter plot bars represent mean +/- SEM. Statistical analysis was performed using a two-tailed Mann–Whitney U-test. *P < 0.05, ns: non-significant.

Figure 3: Specific silencing on mutant allele and protein is maintained over time
A. Semi-quantitative Dnm2 and Atpase RT–PCR products and quantification of Dnm2 expression normalized to *Atpase* (HTZ n≥10, WT n = 12) **B**. EcoNI digestion profile of *Dnm2* PCR products and quantification of the mutant/WT, mutant/*Atpase* and WT/*Atpase* ratios (HTZ, WT n = 11). **C**. DNM2 western blot and quantification of signal by densitometry. GAPDH was used as loading control (HTZ, WT n = 8). Data information: In scatter plots (A, B and C), the bars are mean values and error bars indicate SEM. ***P < 0.001, **P < 0.01, *P < 0.1 two-tailed using a Mann–Whitney U-test comparison. HTZ: heterozygous, WT: wild-type, Mut: Mutant.

Figure 4: DNM2 protein expression in wild-type mouse muscle and non-muscle tissues with aging

A. DNM2 western blot of total protein extracted from tibialis anterior at 1, 3 and 6 months of age and quantification of signal by densitometry. GAPDH was used as loading control (n≥3) **B**. Semi-quantitative *Dnm2* and *Atpase* RT–PCR of mRNA extracted from tibialis anterior muscle at 9 months and quantification of *Dnm2* expression normalized to *Atpase* (n≥3). **C**. DNM2 and GAPDH western blot and total protein stain free extracted from WT brain, liver, quadriceps, gastrocnemius and heart at 1 and 9 months of age. The histograms show quantification of DNM2 protein signal by densitometry using total protein loading (stain free) as loading control (WT-1M n=4, WT-9M n≥3). WT: wild-type. SF: protein stain free. Data information: In scatters blot, bars represent mean ± SEM. Statistical analysis was performed using a two-tailed Mann–Whitney U-test. *P < 0.05.

Figure 5: DNM2 protein expression in healthy human muscle and CNM muscle.

A. Representative DNM2 western blot of total protein extracted from human muscle biopsies. GAPDH and total protein loading was used as loading control. **B**. Histograms showing quantification of DNM2 protein signal by densitometry using total protein loading (stain free) as loading control (<20y n=6, >20y n=6). **C**. Individual plot of densitometry of bands corresponding to DNM2 normalized to total protein stain free as a function of age. Controls patients are represented by black plots (n=12) and CNM patients by red plots (n=5). Individual plot represents mean ±SEM of 1 to 4 technical duplicates. Statistical analysis was performed using spearman correlation (*P < 0.05). SF: protein stain free.

Figure 6: High dose of therapeutic AAV-sh9 does not improve the benefit in old mice

A. Muscle mass relative to body weight in milligrams/grams, absolute maximal force in grams and specific maximal force (in grams/mg) developed by TA muscles from WT and AAV-injected HTZ mice (WT n = 8, HTZ-control n=7 and HTZ-sh9 n=4). **B**. Quantification of *Dnm2* expression normalized to *Atpase* from semi-quantitative *Dnm2* and *Atpase* RT–PCR (left) and quantification of the mutant/WT ratio from EcoNI digestion profile of *Dnm2* PCR (right) (WT ≥ 4, HTZ-Ctl n=4 and HTZ-sh9=4). **C**. Quantification of the viral genomes (vg) per ng of DNA in HTZ 6-month-old mice injected with AAV1-sh9 at low (n = 4) or high dose (n=4). **D**. Representative Haematoxylin–Eosin staining (HE) staining of TA sections from WT and AAV-injected HTZ mice. Data information: In Histogram/scatters blot (A-C), bars represent mean ± SEM. Statistical analysis was performed using Mann–Whitney U-test. *P < 0.05, **P < 0.01 and ***P < 0.001.

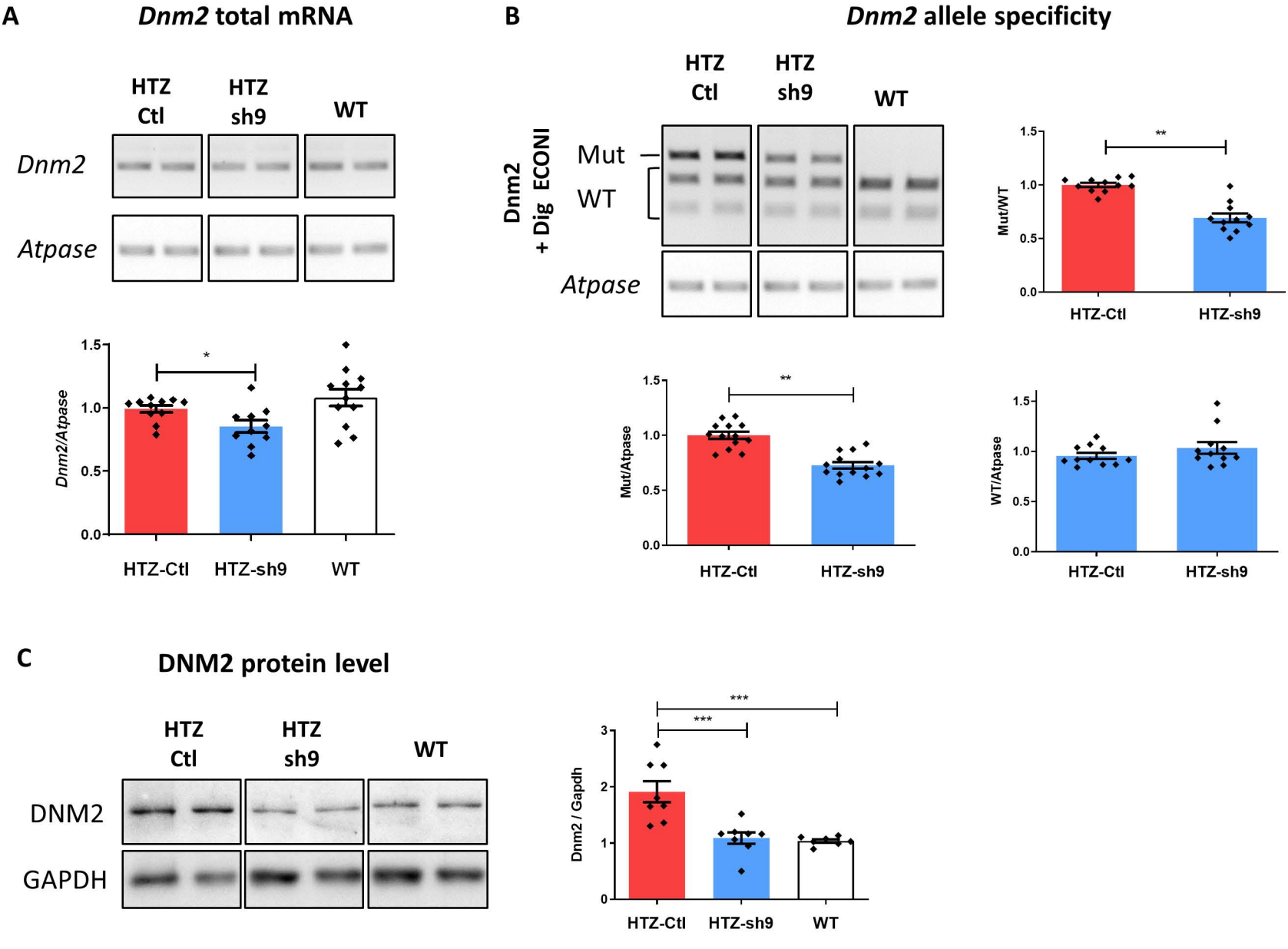
A
Dnm2 total mRNA
HTZ Ctl
HTZ sh9
WT
Dnm2
Atpase
Dnm2/Atpase
HTZ-Ctl
HTZ-sh9
WT
B
Dnm2 allele specificity
Dnm2 + Dig ECONI
Mut
WT
Atpase
Mut/WT
Mut/Atpase
WT/Atpase
C
DNM2 protein level
DNM2
GAPDH
Dnm2 / Gapdh

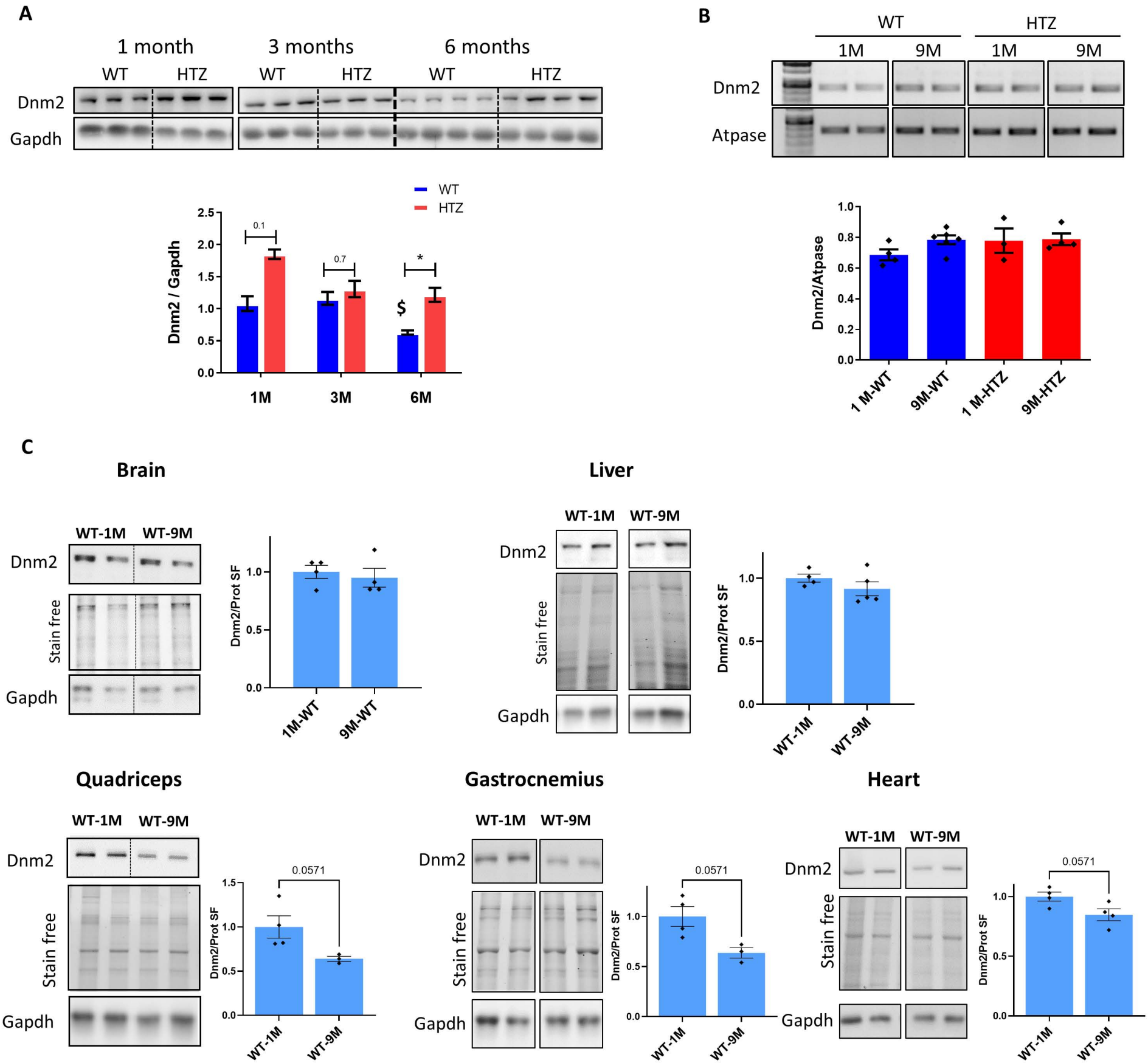
A
1 month
3 months
6 months
WT
HTZ
Dnm2
Gapdh
Dnm2 / Gapdh
0.1
0.7
*
$
1M
3M
6M
B
WT
HTZ
1M
9M
Dnm2
Atpase
Dnm2/Atpase
1 M-WT
9M-WT
1 M-HTZ
9M-HTZ
C
Brain
Liver
Quadriceps
Gastrocnemius
Heart
WT-1M
WT-9M
Stain free
Dnm2/Prot SF
1M-WT
9M-WT
0.0571

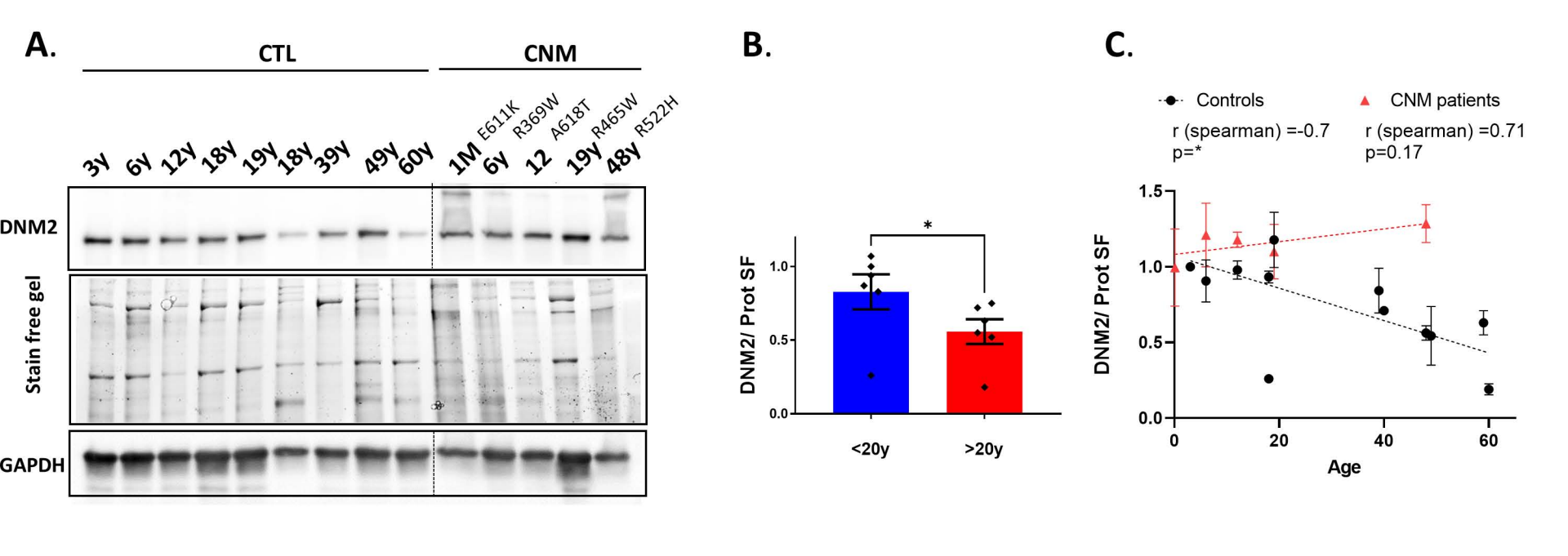
A.
CTL
CNM
3y
6y
12y
18y
19y
18y
39y
49y
60y
1M E611K
6y R369W
12 A618T
19y R465W
48y R522H
DNM2
Stain free gel
GAPDH
B.
DNM2/ Prot SF
1.0
0.5
0.0
*
<20y
>20y
C.
Controls
CNM patients
r (spearman) =-0.7
p=*
r (spearman) =0.71
p=0.17
DNM2/ Prot SF
1.5
1.0
0.5
0.0
0
20
40
60
Age

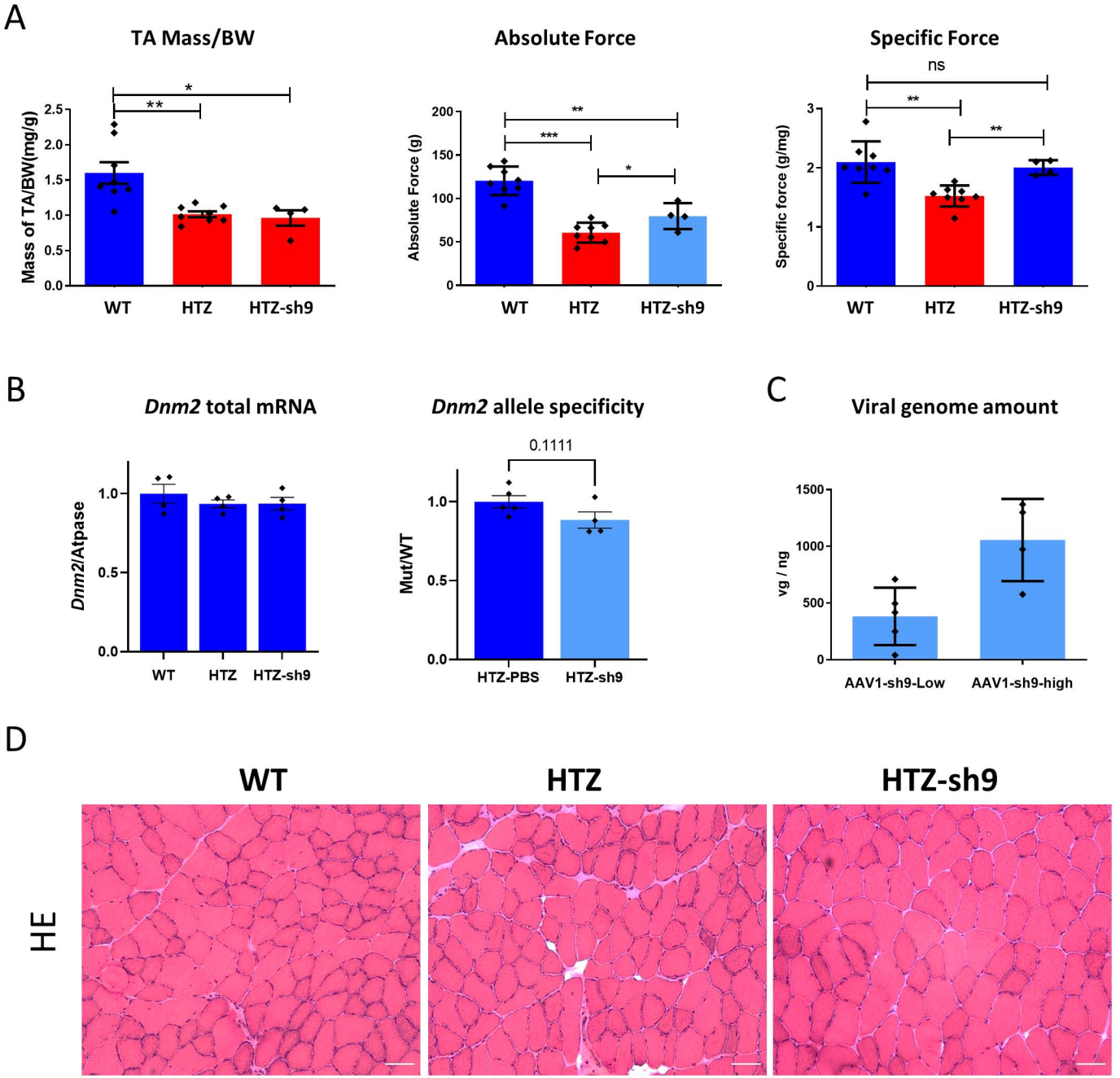
A
TA Mass/BW
Mass of TA/BW(mg/g)
2.5
2.0
1.5
1.0
0.5
0.0
*
**
WT
HTZ
HTZ-sh9
Absolute Force
Absolute Force (g)
200
150
100
50
0
**
***
*
WT
HTZ
HTZ-sh9
Specific Force
Specific force (g/mg)
3
2
1
0
ns
**
**
WT
HTZ
HTZ-sh9
B
Dnm2 total mRNA
Dnm2/Atpase
1.0
0.5
0.0
WT
HTZ
HTZ-sh9
Dnm2 allele specificity
Mut/WT
1.0
0.5
0.0
0.1111
HTZ-PBS
HTZ-sh9
C
Viral genome amount
vg / ng
1500
1000
500
0
AAV1-sh9-Low
AAV1-sh9-high
D
WT
HTZ
HTZ-sh9
HE

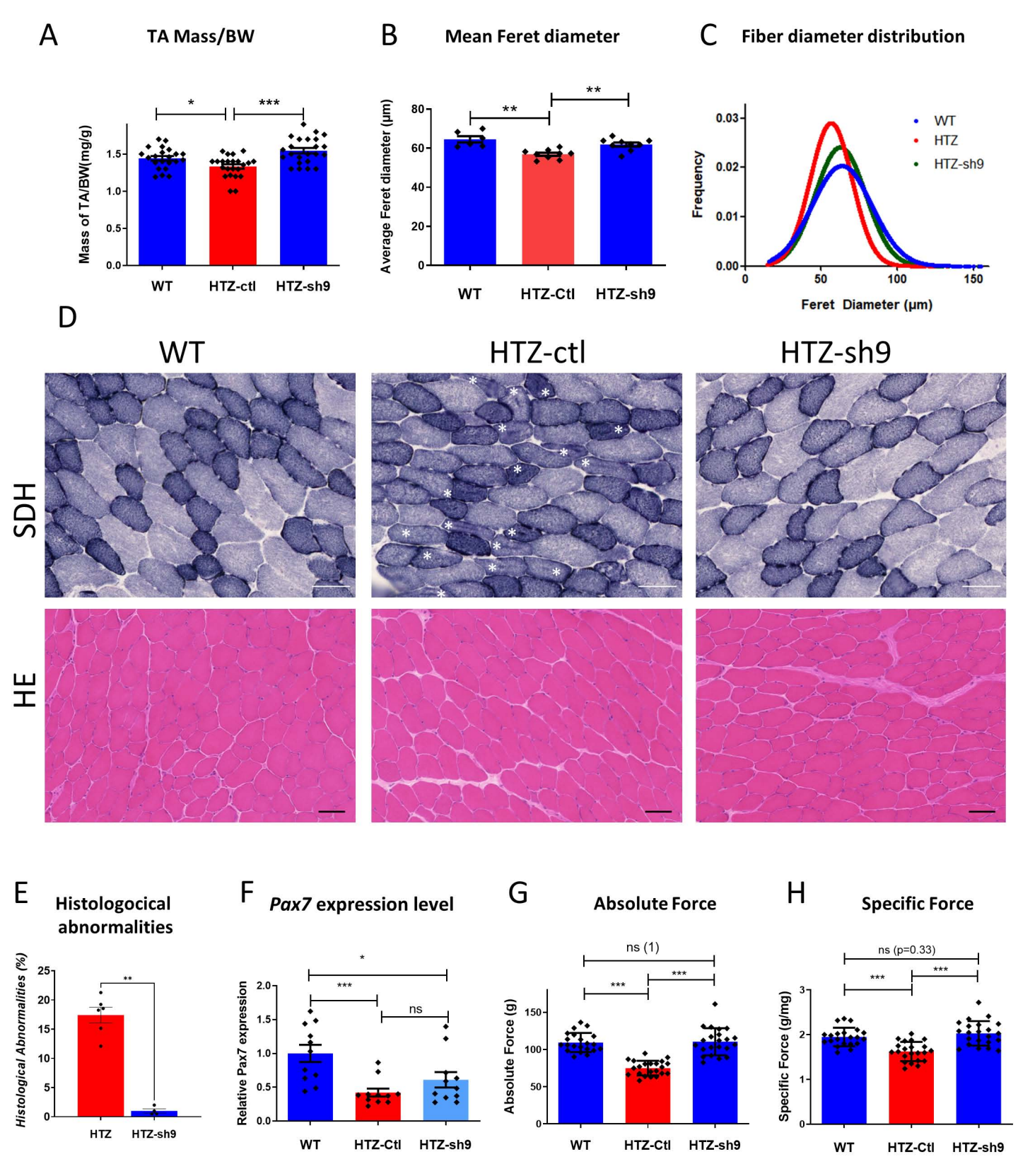
A
TA Mass/BW
Mass of TA/BW(mg/g)
WT
HTZ-ctl
HTZ-sh9
B
Mean Feret diameter
Average Feret diameter (μm)
C
Fiber diameter distribution
Frequency
Feret Diameter (μm)
D
WT
HTZ-ctl
HTZ-sh9
SDH
HE
E
Histologocical abnormalities
Histological Abnormalities (%)
HTZ
HTZ-sh9
F
Pax7 expression level
Relative Pax7 expression
G
Absolute Force
Absolute Force (g)
ns (1)
H
Specific Force
Specific Force (g/mg)
ns (p=0.33)

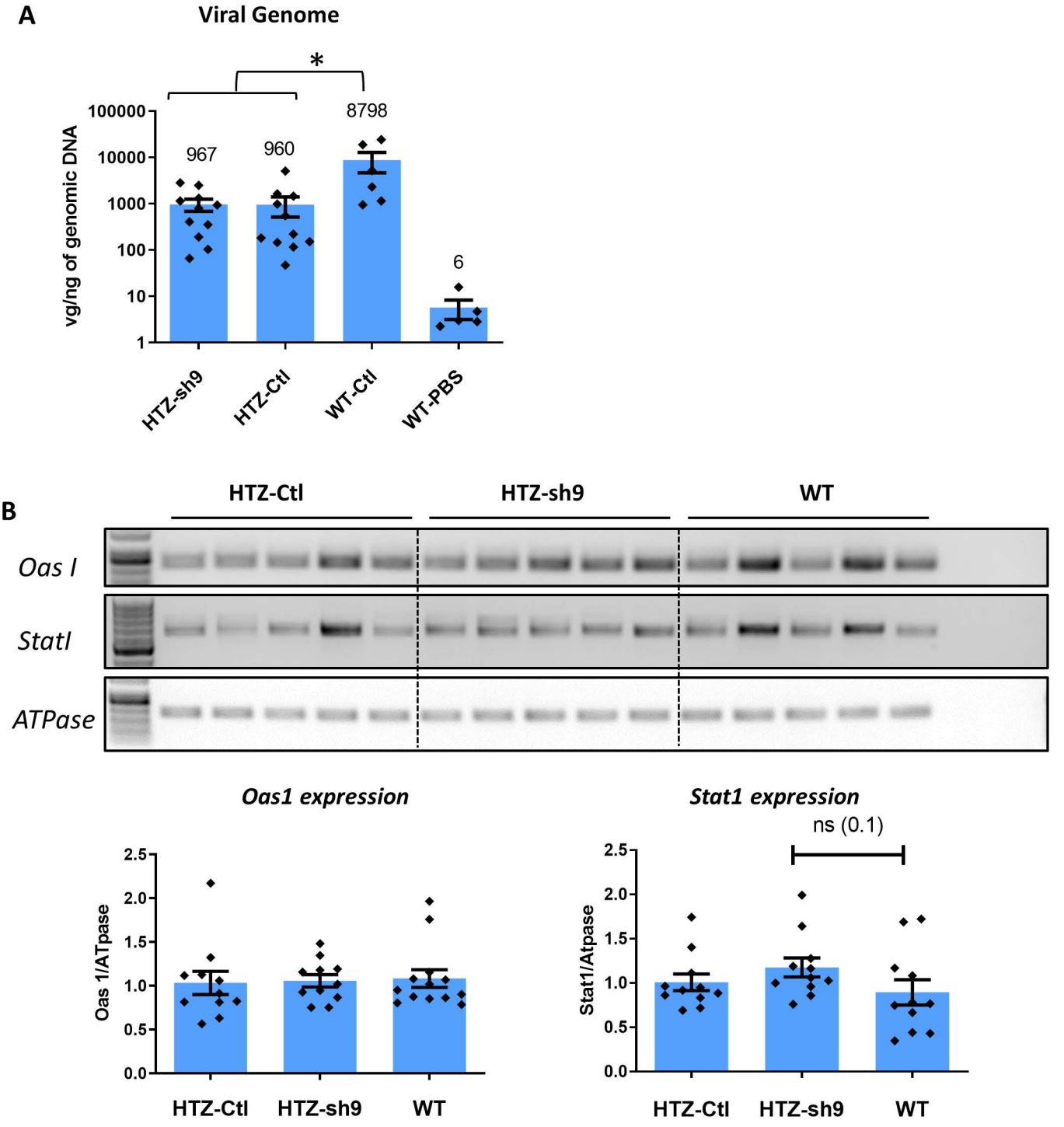
A
Viral Genome
*
vg/ng of genomic DNA
100000
10000
1000
100
10
1
967
960
8798
6
HTZ-sh9
HTZ-Ctl
WT-Ctl
WT-PBS
B
HTZ-Ctl
HTZ-sh9
WT
Oas I
StatI
ATPase
Oas1 expression
Oas 1/ATpase
2.5
2.0
1.5
1.0
0.5
0.0
HTZ-Ctl
HTZ-sh9
WT
Stat1 expression
ns (0.1)
Stat1/Atpase
2.5
2.0
1.5
1.0
0.5
0.0
HTZ-Ctl
HTZ-sh9
WT

Supplemental Data

Table of content

Supplemental Figures

Figure S1

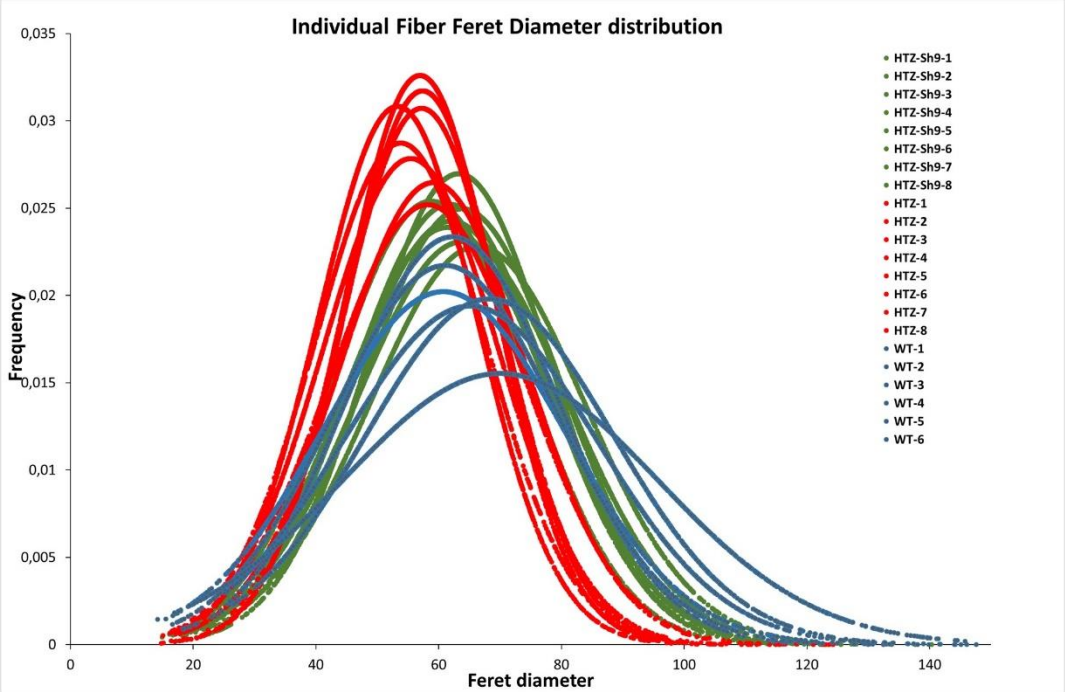

Supplemental Figure S1. Individual Feret diameter distribution. Frequency graph of Feret diameter (µm). WT in blue, HTZ treated in green, HTZ untreated in red.

Figure S2

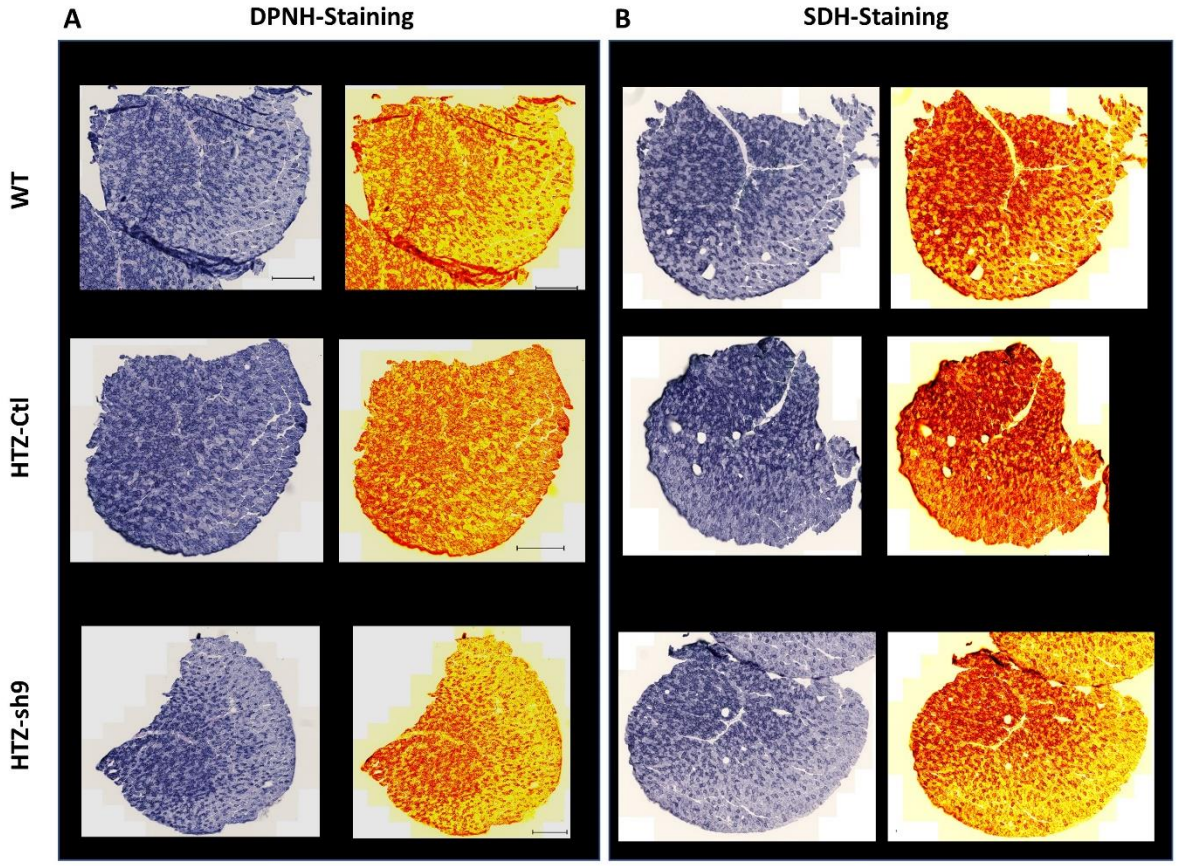

Supplemental Figure S2. Histochemical staining of whole TA sections from WT and AAV-injected HTZ mice. **A.** DPNH: reduced DiphosPhopyridine Nucleotide diaphorase staining **B.** SDH: Succinate DeHydrogenase staining. In A and B left images are real RGB color images, on the right images a Sun LUT is applied. Ctl: control Scale Bar=500 µm.

Figure S3

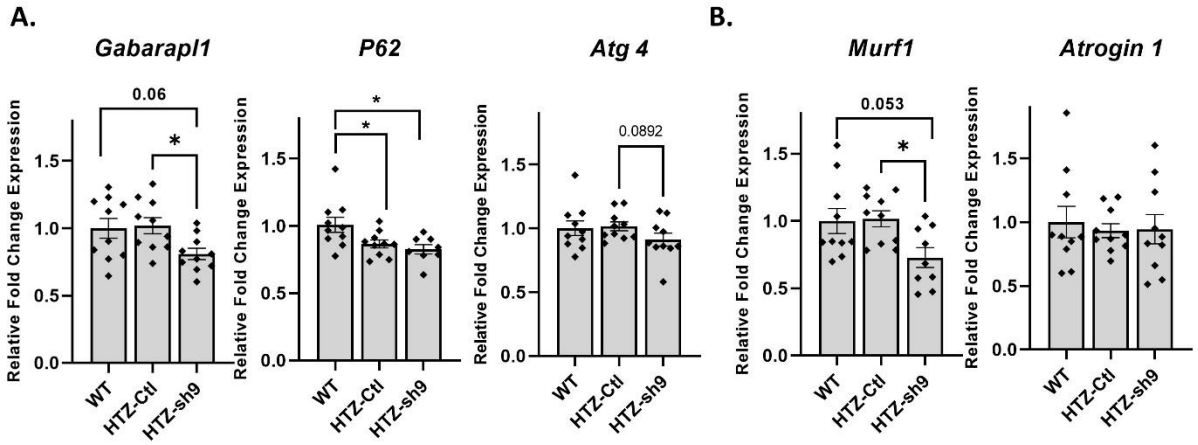

Supplemental Figure S3. mRNA Expression of autophagy-related and E3-ubiquitine Ligase genes. A. Relative mRNA expression of autophagy-related *Gabarapl1, P62 and Atg4* in tibialis anterior muscle from WT, HTZ control and HTZ muscles injected with AAV-sh9. **B**. Relative mRNA expression of *Murf1* and *Atrogin1* in tibialis anterior muscle from WT, HTZ control and HTZ muscles injected with AAV-sh9. In A and B, expression was normalized to ATPase and related to WT expression level. (WT n = 10, HTZ n=10). Bars represent mean ± SEM. Statistical analysis was performed using a two-tailed Mann–Whitney U-test. *P < 0.05.

Figure S4

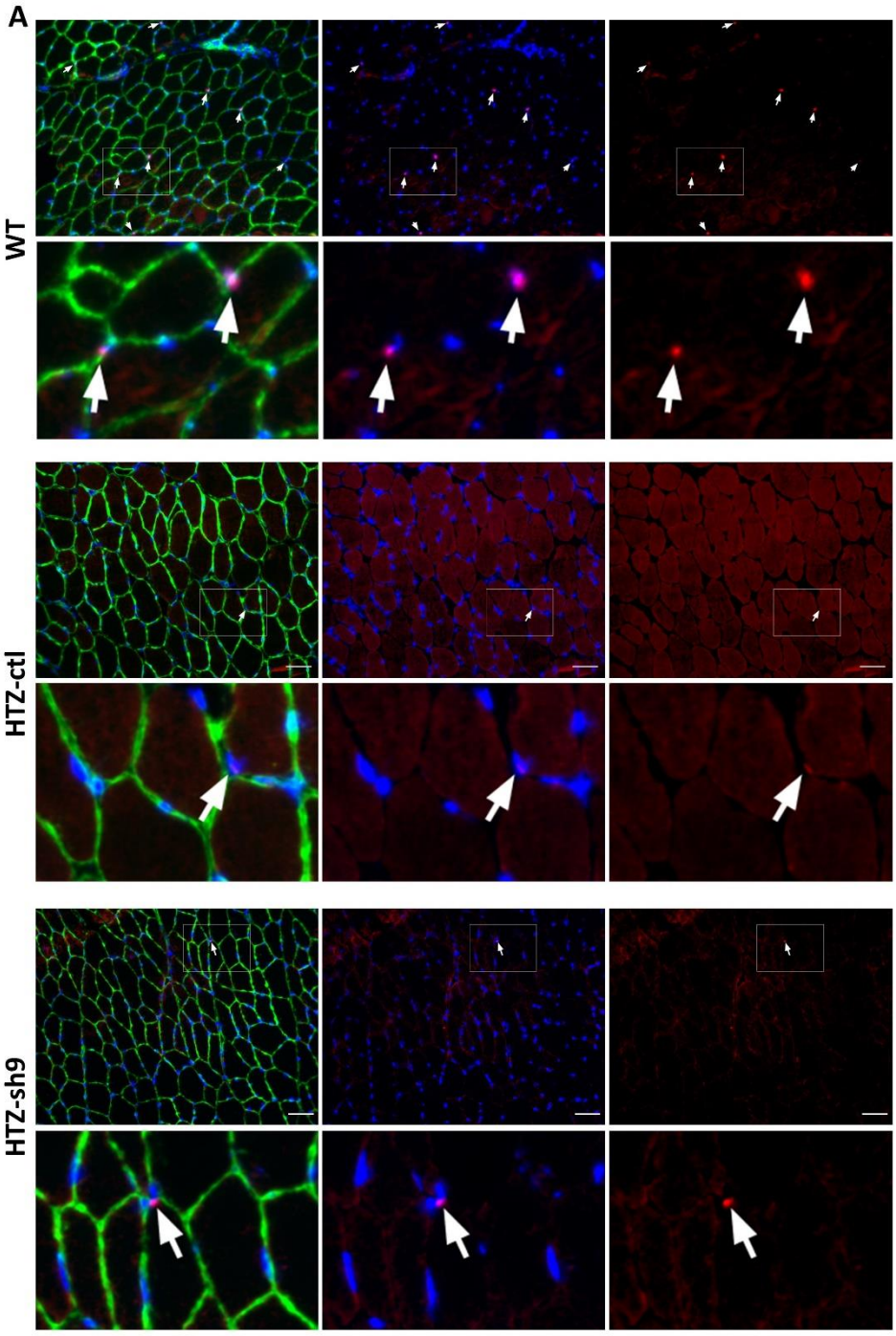
A
WT
HTZ-ctl
HTZ-sh9

B

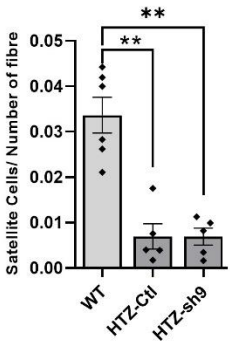
**
**
Satellite Cells/ Number of fibre
0.05
0.04
0.03
0.02
0.01
0.00
WT
HTZ-Ctl
HTZ-sh9

Supplemental Figure S4: Number of satellite cells in TA muscles. A. Representative images of immunostaining in TA muscle at 13months of age in WT and HTZ untreated and treated mice. For each condition, Pax7 (red), Laminin (green) and DAPI (blue) triple staining was illustrated on the left DAPI and Pax7 on the middle and Pax7 alone on the right at low and high magnification (scale bars: 50 µm). Arrows indicates Pax7-positive cells. B. Quantification of the number of satellite cells related to total fibre number in transverse cross-sections. Mean ± sem were indicated on scatter plots. A statistical analysis was performed using a two-tailed Mann–Whitney U-test. **P < 0.01.

Figure S5

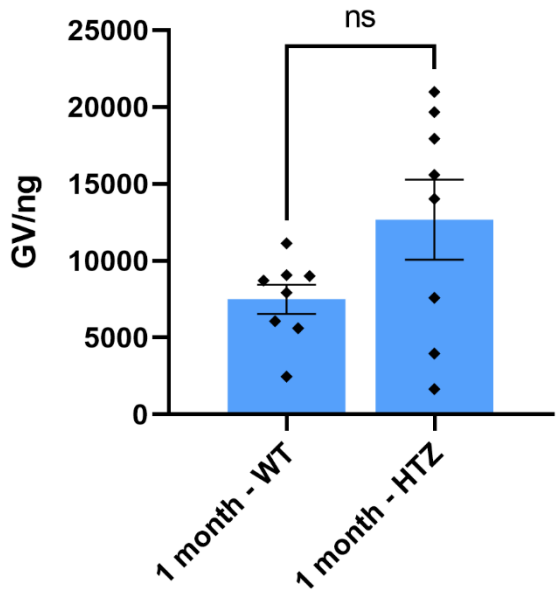

Supplemental Figure S5: Comparison of the viral genomes (vg) between WT and HTZ young mice one month after the injection with AAV1-muSEAP vector. Quantification of the viral genomes (vg)/ ng of DNA in mice injected with AAV-muSEAP (1^{11} vg/TA, (n=8)). Mice were injected at the age of 1 month for a period of 1 month with 1^{11} vg/TA. The scatter plot represents individual values of viral genomes per nucleus. Mean ± SEM are indicated. ns: non significant.

Figure S6

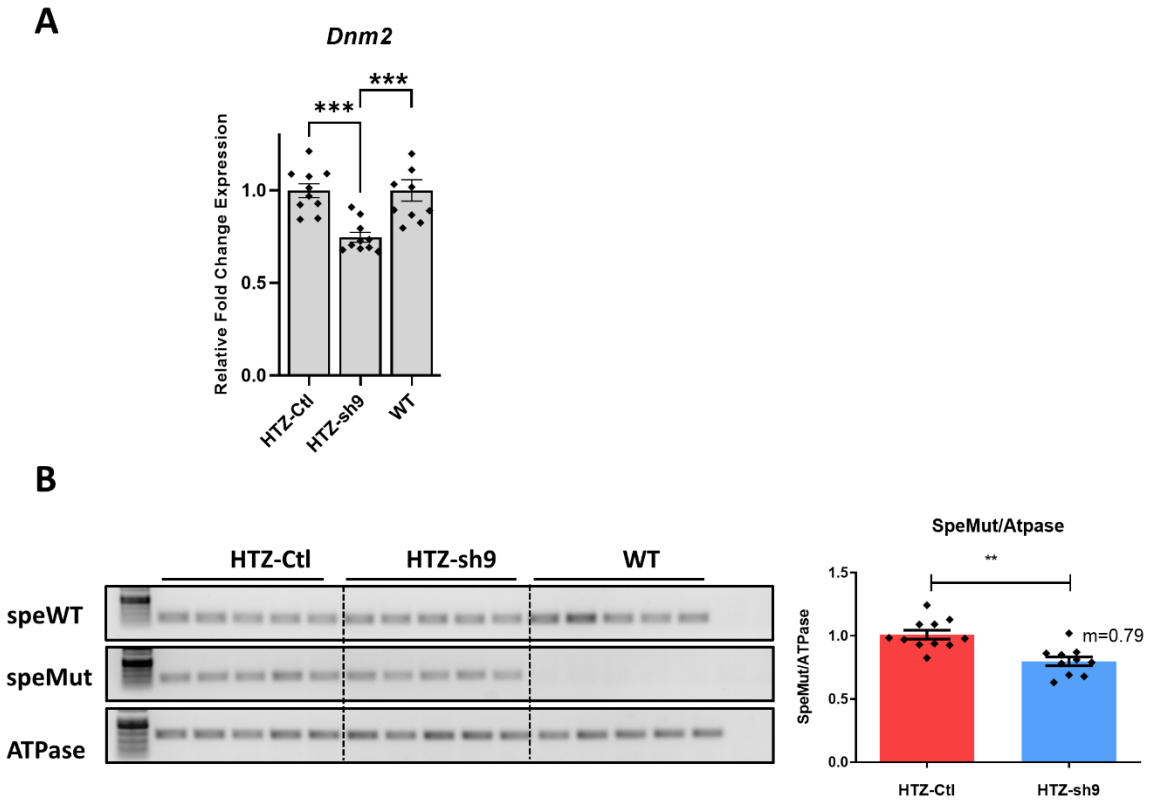

Supplemental Figure S6: Expression of WT and mutated *Dnm2* mRNAs in AAV-transduced mouse muscles. A. Relative *Dnm2* mRNA expression in tibialis anterior muscle from WT, HTZ control and HTZ muscles injected with AAV-sh9. Expression was normalized to ATPase and related to WT expression level. (WT n = 10, HTZ n=10). **B**. Agarose gel electrophoresis and quantification of allele-specific RT-PCR products of Dnm2 mRNAs relative to ATPase. Data information: Bars of the scatter plots represent mean ± SEM.**p<0.01; *** P<0.001 using a two-tailed Mann-Whitney *U*-test (n≥10). Mut: Mutant Dnm2.

Figure S7

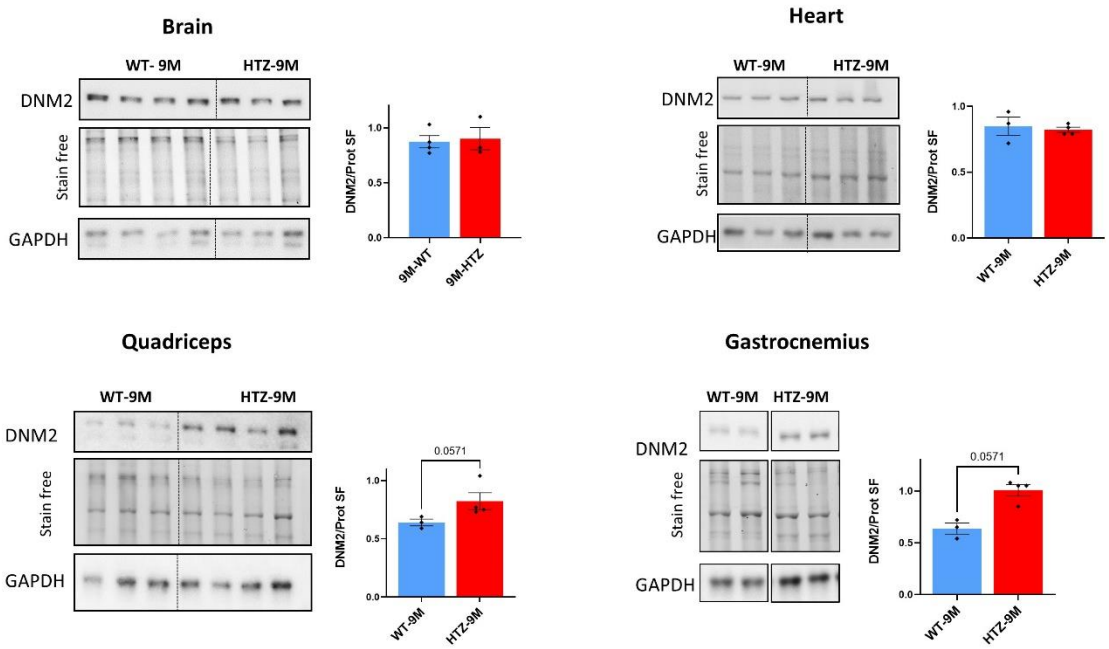

Supplemental Figure S7. Dnm2 protein content in mouse muscle and non-muscle tissues from 9-month-old wild-type and heterozygous mice. DNM2 and GAPDH western blot and total protein extracted from brain, liver, quadriceps, gastrocnemius and heart at 9 months of age (WT-9M n=≥3; HTZ-9M n=4). The histograms show quantification of DNM2 protein signal by densitometry using total protein staining (stain free) as loading control. WT: wild-type, HTZ: heterozygous. SF: stain free. Data information: In scatters blot, bars represent mean ± SEM. Statistical analysis was performed using a two-tailed Mann–Whitney U-test.

Figure S8

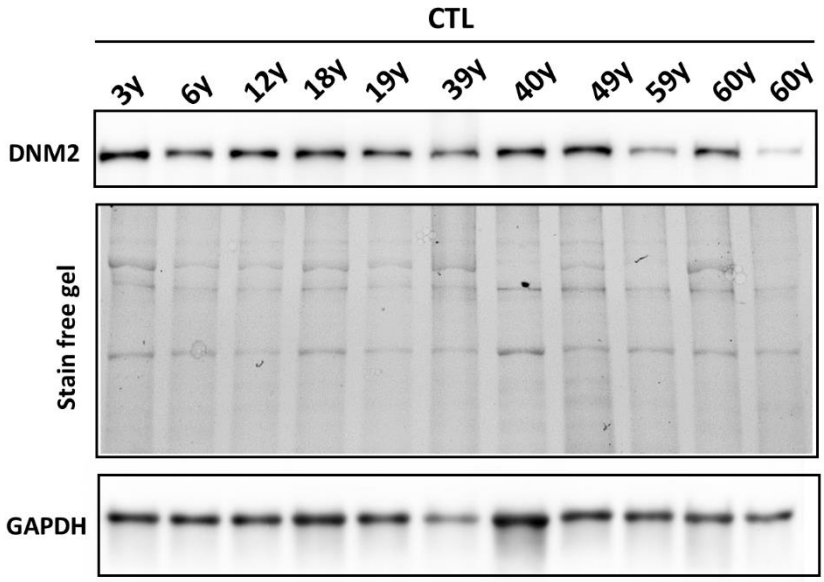

Supplemental Figure S8. Second DNM2 western blot of total protein extracted from human muscle biopsies. GAPDH and total protein staining was used as loading control.